SIAM J. NUMER. ANAL.
Vol. 52, No. 3, pp. 1269–1291

A FINITE VOLUME VENTCELL-SCHWARZ ALGORITHM FOR ADVECTION-DIFFUSION EQUATIONS*

LAURENCE HALPERN† AND FLORENCE HUBERT‡

Abstract. This paper provides a new fully discrete domain decomposition algorithm for the advection diffusion reaction equation. It relies on the optimized Ventcell–Schwarz algorithm with a finite volume discretization of the subdomain problems. The scheme includes a wide range of advection fluxes with a special treatment on the boundary. A complete analysis of the scheme is presented, and the convergence of the algorithm to a discrete approximation of the equation using a modified convective flux is proved. Numerical illustrations of the efficiency of the discrete Ventcell–Schwarz algorithm are given.

Key words. finite volume methods, optimized Schwarz algorithms, Ventcell boundary conditions

AMS subject classifications. 35J25, 65N08, 65N55

DOI. 10.1137/130919799

1. Introduction.

Consider a two-dimensional domain Ω and the boundary value problem

$$\mathcal{L}u := -\mathrm{div}(\nu(x)\nabla u) + \mathrm{div}(\mathbf{b}(x)u) + \eta(x)u = f \tag{1.1}$$

with homogeneous boundary condition $u = 0$ on the boundary $\partial\Omega$.

In today's computational landscape of parallel computers, useful preconditioners for large systems arising from (1.1) in large domains are given by domain decomposition algorithms. To account for difficult geometries and/or large contrast of coefficients, finite volume schemes are widely used in today's industrial codes. The coupling between these two concepts is a crucial issue and not an easy task. This paper presents a new finite volume domain decomposition algorithm, relying on the finite volumes formalism developed in [4] for Robin–Schwarz algorithms and on the efficient Ventcell–Schwarz algorithm first presented in [17].

This algorithm takes its name from the Schwarz algorithm, with transmission between the subdomains given by boundary conditions proposed by Ventcell in [20], who investigated which type of second order boundary conditions would give rise to a strongly continuous semigroup of operators for the Laplace operator. In the last 10 years, interesting interpretations of these boundary conditions have appeared as modeling heat sources on the boundary (called *dynamic boundary conditions* or *permeable walls*); see [15] for the heat equation and [11] for the Cahn–Hilliard equation.

We consider here a nonoverlapping decomposition of Ω into subdomains Ω_j. The Ventcell-Schwarz algorithm approximates u by a sequence of solutions (u_j^n) of (1.1)

*Received by the editors May 6, 2013; accepted for publication (in revised form) February 14, 2014; published electronically June 3, 2014.
http://www.siam.org/journals/sinum/52-3/91979.html
†Laboratoire Analyse, Géométrie et Applications UMR 7539 CNRS, Université Paris 13, 93430 Villetaneuse, France (halpern@math.univ-paris13.fr).
‡LATP, Aix-Marseille Université, 13453 Marseille Cedex 13, France (florence.hubert@univ-amu.fr).

in Ω_j, defined recursively by a transmission condition on the common interface $\Gamma_{i,j} = \partial\Omega_i \cap \partial\Omega_j$:

$$\left(\nu\partial_{n_j} - \frac{1}{2}\mathbf{b}\cdot\mathbf{n}_j + \Lambda\right) u_j^n = \left(-\nu\partial_{n_i} + \frac{1}{2}\mathbf{b}\cdot\mathbf{n}_i + \Lambda\right) u_i^{n-1}. \tag{1.2}$$

The boundary operator Λ involves second order derivatives along the boundary. In the case where $\Gamma_{i,j}$ is a vertical line, it is given by

$$\Lambda\phi = p\phi - q\partial_y(\nu\partial_y\phi) \tag{1.3}$$

with two real parameters p and q. Well-posedness of the boundary value problem is ensured as soon as $p > 0$ and $q \geq 0$. If $q = 0$, Λ reduces to a Robin operator. The coefficients p and q are determined by optimization of the convergence factor in a model case. This process was first described in [17], where the name OO2 was introduced, standing for *optimized of order* 2. Further analysis was conducted in [9], where asymptotic values were given.

The discrete counterpart of the algorithm in the Robin case $q = 0$ was analyzed first in [1] and extended in [5] and [4] in the finite volume framework. For an analysis in the finite element context see [14]. The study of the Ventcell case is, as far as we know, new. It raises new questions that are addressed in this paper.

The first step, in section 2, is to write a finite volume scheme for the discretization of the subdomain problem. It uses a two-point flux approximation for the diffusive flux and a family of discrete convective fluxes as in [6], modified to handle the boundary condition. The convergence of the new Schwarz algorithm toward the approximation of (1.1) in Ω is analyzed in section 3. It is worth noticing that convergence for the discrete algorithm is achieved with a modification of the convective flux at the interface.

Finally, intensive numerical tests show the improvement of the algorithm over the Robin–Schwarz algorithm.

Throughout this paper, the domain Ω is supposed to be bounded and convex. The coefficients p and q in (1.3) are supposed to be positive. These assumptions ensure for the solution u the regularity required for a proper definition of the Ventcell–Schwarz algorithm on the continuous level in section 2.1. (See, however, [7] for a Ventcell–Schwarz algorithm for nonconvex domains in the case of the Laplace operator.) It is also necessary for optimal error estimates in Theorem 2.7, but not for the design of the scheme; see Remark 3.5.

To avoid accumulation of indices, we restrict the presentation to two subdomains only. Since most problems concern regions within subdomains or between two subdomains, the resolution of these can be extended without modifications to the case of many subdomains with any subdomain having at most two neighbors.

2. Finite volume schemes for Ventcell boundary condition. In each subdomain Ω_j, a boundary value problem with mixed boundary conditions must be solved. In this section, the index j is not necessary and will be omitted. Results will next be applied to Ω_j. Thus, consider the advection-diffusion equation in a convex domain Ω with a Dirichlet part Γ^D and a Ventcell part Γ (Γ is assumed to be a vertical segment):

$$\mathcal{L}u := -\mathrm{div}(\nu(x)\nabla u) + \mathrm{div}(\mathbf{b}(x)u) + \eta(x)u = f \text{ in } \Omega, \tag{2.1a}$$

$$u = 0 \text{ on } \Gamma^D, \tag{2.1b}$$

$$\left(\nu\partial_n - \frac{1}{2}\mathbf{b}\cdot\mathbf{n} + \Lambda\right) u = g \text{ on } \Gamma. \tag{2.1c}$$

In a first step, we prove the well-posedness of the problem; then we propose a finite volume scheme for its approximation. Classical fluxes will be used on internal cells, and a special treatment will be applied on the Ventcell part of the boundary.

2.1. Analysis of the boundary value problem.

THEOREM 2.1. *Suppose ν and $\mathbf{b}$ in $W^{1,\infty}(\Omega)$, η in $L^\infty(\Omega)$ and $\nu(x) \geq \bar{\nu} > 0$ for all x in Ω, and $\eta + \frac{1}{2}\mathrm{div}\mathbf{b} \geq 0$ in Ω, $p, q > 0$. For any $(f, g) \in L^2(\Omega) \times L^2(\Gamma)$, problem* (2.1) *admits a unique solution u in*

$$\mathcal{W}_m(\Omega) = \left\{u \in H^2(\Omega) \text{ such that } u = 0 \text{ on } \Gamma^{\mathrm{D}},\ u|_\Gamma \in H^2(\Gamma) \cap H_0^1(\Gamma)\right\}. \tag{2.2}$$

Proof. Write a variational formulation in $H^1_{1,\#}(\Omega) = \{u \in H^1(\Omega), u = 0 \text{ on } \Gamma^D,\ \gamma_\Gamma u \in H_0^1(\Gamma)\}$. Multiply (2.1a) by v and integrate by parts. Introduce

$$\begin{aligned} a_\Omega(u,v) &= \int_\Omega \nu\nabla u\nabla v\, dx\, dy + \frac{1}{2}\int_\Omega ((\mathbf{b}\cdot\nabla u)v - (\mathbf{b}\cdot\nabla v)u)\, dx\, dy \\ &\quad + \int_\Omega \left(\eta + \frac{1}{2}\mathrm{div}\mathbf{b}\right) uv\, dx\, dy, \\ a(u,v) &= a_\Omega(u,v) + \langle \Lambda u, v\rangle_\Gamma. \end{aligned} \tag{2.3}$$

The last term must be understood as a duality product in $H_0^1(\Gamma)$. It may be rewritten in variational form as

$$\langle \Lambda u, v\rangle_\Gamma = p\int_\Gamma uv\, dy + q\int_\Gamma \nu\partial_y u\, \partial_y v\, dy.$$

Λ is a self-adjoint continuous coercive operator from $H_0^1(\Gamma)$ onto $H^{-1}(\Gamma)$. It has a continuous self-adjoint inverse, defining a scalar product on $H^{-1}(\Gamma)$ by

$$\langle u, v\rangle_{\Lambda^{-1}} := \langle v, \Lambda^{-1}u\rangle_\Gamma. \tag{2.4}$$

Computing

$$a(u,u) = \int_\Omega \nu|\nabla u|^2\, dx\, dy + \int_\Omega \left(\eta + \frac{1}{2}\mathrm{div}\mathbf{b}\right)u^2\, dx\, dy + p\int_\Gamma u^2\, dy + q\int_\Gamma \nu(\partial_y u)^2\, dy,$$

it appears that a is a bilinear continuous coercive form on $H^1_{1,\#}(\Omega)$, equipped with the scalar product

$$(w,v)_{H^1_{1,\#}(\Omega)} = (\nabla w, \nabla v)_{L^2(\Omega)} + (\partial_y w, \partial_y v)_{L^2(\Gamma)}. \tag{2.5}$$

This gives existence and uniqueness of a weak solution in $H^1_{1,\#}(\Omega)$, i.e., a solution of

$$a(u,v) = (f,v)_{L^2(\Omega)} + (g,v)_{L^2(\Gamma)}.$$

As for regularity results, u is such that $\Delta u \in L^2(\Omega)$, $u = 0$ on Γ^D, and $(\partial_x - \partial_{yy})u \in L^2(\Gamma)$. Such a regularity result was proved in [19] for a regular boundary with Ventcell boundary condition all over. Due to the convexity of the domain, the result applies here. ∎

2.2. Meshes. The definition of the meshes is introduced here; see [10, 5] for the standard part of the notation. First an admissible mesh in a single domain is defined. Then it is used to create a composite mesh in $\Omega = \Omega_1 \cup \Omega_2$.

2.2.1. Admissible meshes. In this paragraph, the index j is omitted, considering a general open polygonal set Ω. Define a family $\mathfrak{M}$ of polygonal control volumes such that $\bar{\Omega} = \cup_{\mathrm{K}\in\mathfrak{M}}\bar{\mathrm{K}}$ with $\mathrm{K}\cap\mathrm{L} = \emptyset$ if $\mathrm{K} \neq \mathrm{L}$. $\mathfrak{M}$ is an *admissible finite volume mesh* if there exists a family of points $(\boldsymbol{x}_\mathrm{K})_{\mathrm{K}\in\mathfrak{M}}$ that satisfies $(\boldsymbol{x}_\mathrm{K}, \boldsymbol{x}_\mathrm{L}) \perp \sigma$ if $\sigma = \partial\mathrm{K}\cap\partial\mathrm{L}$. If all control volumes K are triangles, the family of triangle circumcenters satisfies this orthogonality condition. The set of all edges σ of control volumes is denoted by $\boldsymbol{\mathcal{E}}$. It is divided into three sets: the edges located inside the domain Ω, $\boldsymbol{\mathcal{E}}_{int} = \{\sigma \in \boldsymbol{\mathcal{E}},\ \sigma = \partial\mathrm{K}\cap\partial\mathrm{L}\}$, the edges $\boldsymbol{\mathcal{E}}_D$ located on the Dirichlet boundary Γ^D, and the edges $\boldsymbol{\mathcal{E}}_\Gamma$ located on the Ventcell boundary Γ. Finally, for any K in $\mathfrak{M}$, $\boldsymbol{\mathcal{E}}_\mathrm{K}$ stands for the edges of its boundary $\partial\mathrm{K}$.

For any $\sigma \in \boldsymbol{\mathcal{E}}_\mathrm{K}$, $\mathbf{n}_{\mathrm{K}\sigma}$ is the outward-pointing unit vector orthogonal to σ, $d_{\mathrm{K},\sigma}$ the signed distance from $\boldsymbol{x}_\mathrm{K}$ to σ ($d_{\mathrm{K},\sigma} > 0$ if $\boldsymbol{x}_\mathrm{K} \in \mathrm{K}$, $d_{\mathrm{K},\sigma} \leq 0$ else), $d_\sigma = d_{\mathrm{K},\sigma}$ if $\sigma \in \boldsymbol{\mathcal{E}}_D \cup \boldsymbol{\mathcal{E}}_\Gamma$, and $d_\sigma = d_{\mathrm{K},\sigma} + d_{\mathrm{L},\sigma}$ is the distance between $\boldsymbol{x}_\mathrm{K}$ and $\boldsymbol{x}_\mathrm{L}$ if $\sigma = \partial\mathrm{K}\cap\partial\mathrm{L} \in \boldsymbol{\mathcal{E}}_{int}$. We assume that $d_\sigma > 0$ for any $\sigma \in \boldsymbol{\mathcal{E}}$, which ensures that the mesh is a Delaunay mesh [10].

Let $|\boldsymbol{\mathcal{E}}_\Gamma|$ be the cardinality of $\boldsymbol{\mathcal{E}}_\Gamma$, and the edges of $\boldsymbol{\mathcal{E}}_\Gamma$ are reordered as $\{\sigma_i\}$, with $\sigma_i \cap \sigma_{i+1}$ reduced to a single point denoted by $x_{i+\frac{1}{2}}$. The control volume in $\mathfrak{M}$ associated to σ_i is denoted by K_i.

For each $\mathrm{K} \in \mathfrak{M}$ or $\sigma \subset \Gamma$, $|\mathrm{K}|$, and $|\sigma|$ denote the two-dimensional measure of K, respectively, the one-dimensional measure of σ.

The full admissible finite volume mesh for the boundary value problem is $\mathcal{T} = \mathfrak{M} \cup \boldsymbol{\mathcal{E}}_\Gamma$. The size of the mesh and its regularity are measured by

$$\mathrm{size}(\mathfrak{M}) = \max_{\mathfrak{M}}(\mathrm{diam}(\mathrm{K})), \quad \mathrm{reg}(\mathcal{T}) = \max_{\mathfrak{M}} \max_{\boldsymbol{\mathcal{E}}_\mathrm{K}} \left\{ \frac{\mathrm{diam}(\mathrm{K})}{|d_{\mathrm{K}\sigma}|} \right\}. \tag{2.6}$$

Figure 1 summarizes this notation. Note that in the case where $\Gamma = \emptyset$, $\boldsymbol{\mathcal{E}}_\Gamma$ is empty, and therefore $\mathcal{T} = \mathfrak{M}$.

2.2.2. Composite meshes. Let us now consider a domain Ω decomposed into two subdomains $\Omega = \Omega_1 \cup \Omega_2$. Assume that the subdomains Ω_j are endowed with

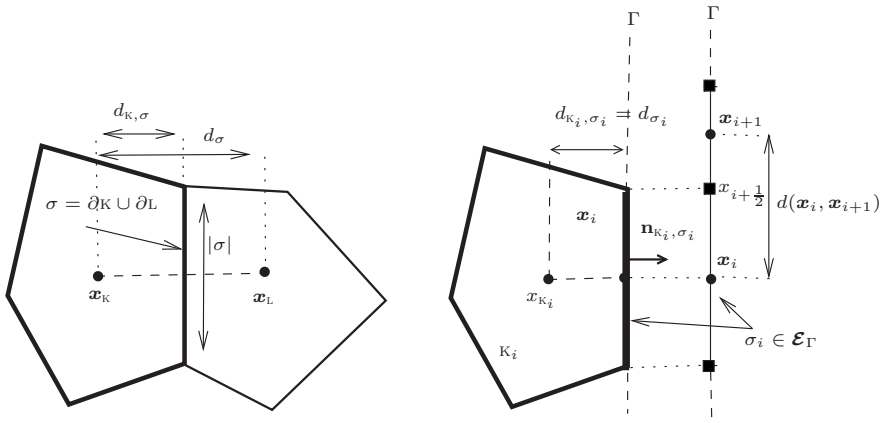

FIG. 1. *Notation for an admissible mesh.*

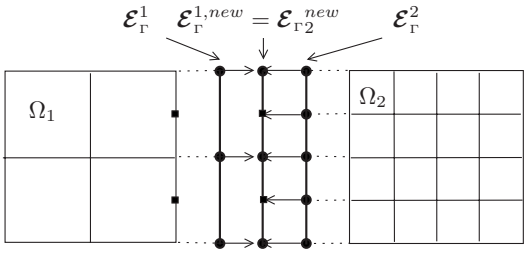

FIG. 2. *Composite mesh.*

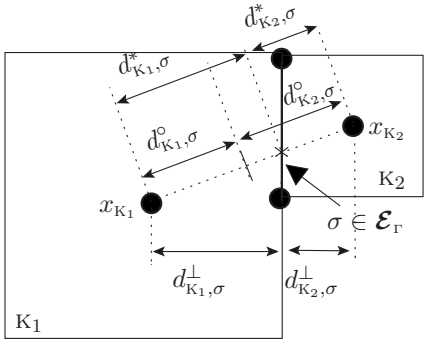

FIG. 3. *Definition of distances* $d_{K_j,\sigma}$ *for* $\sigma \in \mathcal{E}_\Gamma$.

admissible meshes $\mathcal{T}_j = \mathfrak{M}_j \cup \mathcal{E}_\Gamma^j$. The two meshes $\mathcal{T}_1$ and $\mathcal{T}_2$ may correspond to identical meshes on Γ ($\mathcal{E}_\Gamma^1 = \mathcal{E}_\Gamma^2$; see Grid #1 in Figure 7) or not ($\mathcal{E}_\Gamma^1 \neq \mathcal{E}_\Gamma^2$; see Grid #2 in Figure 7). When $\mathcal{E}_\Gamma^1 = \mathcal{E}_\Gamma^2$, the two meshes are said to be *compatible*. In the second case, the meshes can be made compatible by redefining the notion of edges on Γ (see Figure 2) such that

$$\mathcal{E}_\Gamma^{1,new} = \mathcal{E}_\Gamma^{2,new} = \mathcal{E}_\Gamma := \{\sigma = \partial K_1 \cap \partial K_2 \text{ with } K_i \in \mathfrak{M}_i\}. \tag{2.7}$$

In this case, for $\sigma = \partial K_1 \cap \partial K_2 \in \mathcal{E}_\Gamma$, defining $d_{K_j,\sigma}$ requires some care. Several choices are valid (see Figure 3): either the orthogonal distance $d^\perp_{K_j,\sigma}$ between $\boldsymbol{x}_{K_j}$ and Γ, the distance $d^*_{K_j,\sigma}$ between $\boldsymbol{x}_{K_j}$ and the point $\boldsymbol{x}_\sigma$, the intersection between $(\boldsymbol{x}_{K_1}, \boldsymbol{x}_{K_2})$ and Γ, or the half distance $d^\circ_{K_j,\sigma}$ between $\boldsymbol{x}_{K_1}$ and $\boldsymbol{x}_{K_2}$. Note that we only require that $d_{K_j,\sigma} = d^\perp_{K_j,\sigma}(1 + \mathcal{O}(\text{size}(\mathfrak{M}_j))$.

Finally a *composite mesh* associated to $\Omega = \Omega_1 \cup \Omega_2$ is a quintuplet $\mathcal{T} = (\mathfrak{M}, \mathfrak{M}_1, \mathcal{E}_\Gamma^1, \mathfrak{M}_2, \mathcal{E}_\Gamma^2)$ such that each mesh $\mathfrak{M}_j$ is an admissible mesh for Ω_j, $\mathfrak{M}_1$ and $\mathfrak{M}_2$ are compatible, i.e., $\mathcal{E}_\Gamma^1 = \mathcal{E}_\Gamma^2 = \mathcal{E}_\Gamma$, and $\mathfrak{M} := \mathfrak{M}_1 \cup \mathfrak{M}_2$.

2.3. The classical two-point flux approximation. Let $\mathfrak{M}$ be an admissible mesh of Ω and $\mathbf{u}^{\mathfrak{M}} = (u_K)_{K \in \mathfrak{M}}$. The discrete volume equation is obtained by integrating (1.1) over each control volume K and by approximating the resulting normal fluxes as follows. Integrate (1.1) over the control volume K to get

$$\sum_{\sigma \in \mathcal{E}_K} \left(-\int_\sigma \nu \nabla u \cdot \mathbf{n}_{K\sigma}\, ds + \int_\sigma \mathbf{b} \cdot \mathbf{n}_{K\sigma} u\, ds \right) + \int_K \eta u\, d\boldsymbol{x} = \int_K f(\boldsymbol{x}) d\boldsymbol{x}.$$

The volume term $\int_K \eta u\, d\boldsymbol{x}$ is approximated by $\eta_K u_K$ with $\eta_K = \frac{1}{|K|}\int_K \eta$. The total flux over the boundary of K is the sum on the edges of the diffusive flux $-\int_\sigma \nu \nabla u \cdot \mathbf{n}_{K\sigma}\, ds$

and the convective flux $\int_\sigma \mathbf{b}\cdot\mathbf{n}_{\mathrm{K}\sigma} u\,ds$. They are approximated by the discrete fluxes $F^d_{\mathrm{K},\sigma}$ and $F^c_{\mathrm{K},\sigma}$ to be defined below. Defining the total discrete flux on the edge σ as $F_{\mathrm{K},\sigma} = F^d_{\mathrm{K},\sigma} + F^c_{\mathrm{K},\sigma}$, (1.1) in Ω is discretized by

$$\forall \mathrm{K}\in\mathfrak{M},\quad \sum_{\sigma\in\boldsymbol{\mathcal{E}}_{\mathrm{K}}} F_{\mathrm{K},\sigma} + |\mathrm{K}|\eta_{\mathrm{K}} u_{\mathrm{K}} = \int_{\mathrm{K}} f(\boldsymbol{x})\,d\boldsymbol{x}. \tag{2.8}$$

We use the classical diffusive discrete fluxes

$$F^d_{\mathrm{K},\sigma} = |\sigma|\nu_\sigma \frac{u_{\mathrm{K}} - \widetilde{u}_\sigma}{d_\sigma} \text{ with } \widetilde{u}_\sigma = \begin{cases} u_{\mathrm{L}} & \text{if } \sigma = \partial\mathrm{K}\cap\partial\mathrm{L}\in\boldsymbol{\mathcal{E}}_{int},\\ 0 & \text{if } \sigma\in\boldsymbol{\mathcal{E}}_D, \end{cases} \tag{2.9}$$

where $\nu_\sigma = \frac{1}{|\sigma|}\int_\sigma \nu(s)\,ds$ or $\nu_\sigma = \nu(x_\sigma)$ (x_σ center of σ).

We use the family of discrete advection fluxes introduced in [6] (with a slight change of notation),

$$F^c_{\mathrm{K},\sigma} = \frac{1}{2}|\sigma| b_{\mathrm{K}\sigma}(u_{\mathrm{K}} + \widetilde{u}_\sigma) + \frac{|\sigma|\nu_\sigma}{d_\sigma} B_\sigma\left(\frac{d_\sigma b_{\mathrm{K}\sigma}}{\nu_\sigma}\right)(u_{\mathrm{K}} - \widetilde{u}_\sigma), \tag{2.10}$$

where $b_{\mathrm{K}\sigma} = \frac{1}{|\sigma|}\int_\sigma \mathbf{b}\cdot\mathbf{n}_{\mathrm{K}\sigma}\,ds$, and for any edge σ, B_σ is an even Lipschitz continuous function such that

$$B_\sigma(0) = 0 \text{ and } \exists\, \underline{c} > 0\ \forall\sigma\in\boldsymbol{\mathcal{E}},\ \forall s\in\mathbb{R},\ B_\sigma(s) + 1 > \underline{c} > 0. \tag{2.11}$$

These schemes thus appear as stabilization of the centered scheme. All the classical schemes belong to this family. The centerd scheme corresponds to $B_\sigma(s) = B^c(s) = 0$, the upwind scheme to $B_\sigma(s) = B^{up}(s) = \frac{1}{2}|s|$, and the Scharfetter–Gummel scheme to $B_\sigma(s) = B^{SG}(s) = \frac{1}{2}(\frac{s}{e^s-1} - \frac{s}{e^{-s}-1}) - 1$.

The well-posedness and convergence of the scheme (2.8)–(2.9)–(2.10) with Dirichlet boundary conditions is now classical; see [10, 6].

Remark 2.2. Assume that $\mathcal{T} = (\mathfrak{M}, \mathfrak{M}_1, \mathfrak{M}_2, \boldsymbol{\mathcal{E}}^1_\Gamma, \boldsymbol{\mathcal{E}}^2_\Gamma)$ is a composite mesh. The mesh $\mathfrak{M}$ is a discretization of Ω that may present nonadmissible edges located on Γ (see Figure 3 or 7), i.e., the orthogonality condition for $\sigma\in\boldsymbol{\mathcal{E}}_\Gamma$ is lost. In that case we can still obtain an error estimate in size$(\mathfrak{M})^{\frac{1}{2}}$ (see [5]) instead of the classical size$(\mathfrak{M})$.

2.4. A two-point flux approximation for Ventcell boundary conditions. In order to take into account the Ventcell boundary condition (2.1c), a new set of unknowns is needed on the edges on Γ, namely, $\mathbf{u}^{\boldsymbol{\mathcal{E}}_\Gamma} = (u_\sigma)_{\sigma\in\boldsymbol{\mathcal{E}}_\Gamma}$. Then the full vector of unknowns is $\mathbf{u}^{\mathcal{T}} = (\mathbf{u}^{\mathfrak{M}}, \mathbf{u}^{\boldsymbol{\mathcal{E}}_\Gamma})$. A new discrete equation is obtained by integrating the Ventcell boundary condition (2.1c) over the boundary control cell $\sigma_i\in\boldsymbol{\mathcal{E}}_\Gamma$:

$$\int_{\sigma_i} \nu\nabla u\cdot\mathbf{n}_{\mathrm{K}_i\sigma_i}\,ds - \frac{1}{2}\int_{\sigma_i}\mathbf{b}\cdot\mathbf{n}_{\mathrm{K}_i\sigma_i} u\,ds + p\int_{\sigma_i} u\,ds + q\,[-\nu\partial_y u]^{\boldsymbol{x}_{i+\frac{1}{2}}}_{\boldsymbol{x}_{i-\frac{1}{2}}} = \int_{\sigma_i} g_j(s)\,ds. \tag{2.12}$$

Approximate the term $-\int_{\sigma_i}\nu\nabla u\cdot\mathbf{n}_{\mathrm{K}_i\sigma_i}\,ds + \int_{\sigma_i}\mathbf{b}\cdot\mathbf{n}_{\mathrm{K}_i\sigma_i}u\,ds$ by $F_{\mathrm{K}_i,\sigma_i}$ and then the sum of the first two terms in (2.12) by $-F_{\mathrm{K}_i,\sigma_i} + \frac{1}{2}b_{\mathrm{K}_i\sigma_i}|\sigma_i|u_{\sigma_i}$. Define the discrete one-dimensional flux $F_{i+\frac{1}{2}}$ as an approximation of $-\nu\partial_y u(\boldsymbol{x}_{i+\frac{1}{2}})$, given by

$$F_{i+\frac{1}{2}} = -\nu(x_{i+\frac{1}{2}})\frac{u_{\sigma_{i+1}} - u_{\sigma_i}}{d(\boldsymbol{x}_{i+1},\boldsymbol{x}_i)} \quad \text{for } i = 0,\dots,|\boldsymbol{\mathcal{E}}^j_\Gamma|, \tag{2.13}$$

with the convention $u_{\sigma_0} = 0$ and $u_{\sigma_{|\boldsymbol{\mathcal{E}}_\Gamma|+1}} = 0$.

Define the total flux $F_{\mathrm{K}\sigma}$ by (2.9), (2.10) with a modification on the boundary Γ:

$$\tilde{u}_\sigma = \begin{cases} u_{\mathrm{L}} & \text{if } \sigma = \partial\mathrm{K} \cap \partial\mathrm{L} \in \boldsymbol{\mathcal{E}}_{int}, \\ 0 & \text{if } \sigma \in \boldsymbol{\mathcal{E}}_D, \\ u_\sigma & \text{if } \sigma \in \boldsymbol{\mathcal{E}}_\Gamma. \end{cases} \tag{2.14}$$

Define the discrete boundary operator Λ_Γ by

$$(\Lambda_\Gamma \mathbf{u}^{\boldsymbol{\mathcal{E}}_\Gamma})_\sigma = p|\sigma|u_\sigma - q(F_{i+\frac{1}{2}} - F_{i-\frac{1}{2}}) \text{ if } \sigma = \sigma_i. \tag{2.15}$$

The full discrete system involving the volume and boundary unknowns is

$$\forall \mathrm{K} \in \mathfrak{M}, \qquad \sum_{\sigma \in \boldsymbol{\mathcal{E}}_\mathrm{K}} F_{\mathrm{K},\sigma} + |\mathrm{K}|\eta_\mathrm{K} u_\mathrm{K} = \int_\mathrm{K} f(\boldsymbol{x})\, d\boldsymbol{x}, \tag{2.16}$$

$$\forall \sigma \in \boldsymbol{\mathcal{E}}_\Gamma, \qquad -F_{\mathrm{K},\sigma} + \frac{1}{2} b_{\mathrm{K}\sigma} m_\sigma u_\sigma + (\Lambda_\Gamma \mathbf{u}^{\boldsymbol{\mathcal{E}}_\Gamma})_\sigma = \int_\sigma g(s)\, ds. \tag{2.17}$$

2.5. Discrete norms. The discrete vectors $\mathbf{u}^{\mathfrak{M}}$ and $\mathbf{u}^{\boldsymbol{\mathcal{E}}_\Gamma}$ can be identified as piecewise constant functions $u^{\mathfrak{M}}$ and $u^{\boldsymbol{\mathcal{E}}_\Gamma}$ on Ω and Γ, respectively, with L^2 norms $\|\mathbf{u}^{\mathfrak{M}}\|_{0,\Omega}$, $\|\mathbf{u}^{\boldsymbol{\mathcal{E}}_\Gamma}\|_{0,\Gamma}$. Discrete H^1 norms can also be associated to these vectors by

$$\|\mathbf{u}^{\mathfrak{M}}\|_{1,\mathfrak{M}} = \left(\sum_{\sigma \in \boldsymbol{\mathcal{E}}_{int}} |\sigma| \frac{|u_\mathrm{K} - u_\mathrm{L}|^2}{d_\sigma} + \sum_{\sigma \in \boldsymbol{\mathcal{E}}_D} |\sigma| \frac{|u_\mathrm{K}|^2}{d_\sigma} \right)^{\frac{1}{2}}, \tag{2.18}$$

$$\|\mathbf{u}^{\mathcal{T}}\|_{1,\mathcal{T}} = \left(\sum_{\sigma \in \boldsymbol{\mathcal{E}}_{int}} |\sigma| \frac{|u_\mathrm{K} - u_\mathrm{L}|^2}{d_\sigma} + \sum_{\sigma \in \boldsymbol{\mathcal{E}}_D} |\sigma| \frac{|u_\mathrm{K}|^2}{d_\sigma} + \sum_{\sigma \in \boldsymbol{\mathcal{E}}_\Gamma} |\sigma| \frac{|u_\mathrm{K} - u_\sigma|^2}{d_\sigma} \right)^{\frac{1}{2}}, \tag{2.19}$$

$$\|\mathbf{u}^{\boldsymbol{\mathcal{E}}_\Gamma}\|_{1,\boldsymbol{\mathcal{E}}_\Gamma} = \left(\sum_{i=0}^{|\boldsymbol{\mathcal{E}}_\Gamma|} \frac{|u_{\sigma_{i+1}} - u_{\sigma_i}|^2}{d(x_{i+1}, x_i)} \right)^{\frac{1}{2}}. \tag{2.20}$$

Discrete Poincaré (provided Γ^d is not empty) and trace inequalities have been proved in [10]:

(2.21)
$$\|\mathbf{u}^{\mathfrak{M}}\|_{0,\Omega} \le C\|\mathbf{u}^{\mathfrak{M}}\|_{1,\mathfrak{M}},\ \|\mathbf{u}^{\mathfrak{M}}\|_{0,\Omega} + \|\mathbf{u}^{\boldsymbol{\mathcal{E}}_\Gamma}\|_{0,\Gamma} \le C\|\mathbf{u}^{\mathcal{T}}\|_{1,\mathcal{T}},\ \|\mathbf{u}^{\boldsymbol{\mathcal{E}}_\Gamma}\|_{0,\Gamma} \le C\|\mathbf{u}^{\boldsymbol{\mathcal{E}}_\Gamma}\|_{1,\boldsymbol{\mathcal{E}}_\Gamma}.$$

2.6. Properties of the scheme.

LEMMA 2.3 (A first a priori estimate). *For any* $\mathbf{u}^{\mathfrak{M}} = (u_\mathrm{K})_{\mathrm{K}\in\mathfrak{M}}$, *solution of* (2.16),

$$\begin{aligned} &\sum_{\mathrm{K}\in\mathfrak{M}} \sum_{\sigma\in\boldsymbol{\mathcal{E}}_\mathrm{K}} \frac{|\sigma|\nu_\sigma}{d_\sigma} (1 + B_\sigma) |u_\mathrm{K} - \tilde{u}_\sigma|^2 + \int_\Omega \left(\eta + \frac{1}{2}\mathrm{div}\mathbf{b} \right) |u^{\mathfrak{M}}|^2 \\ &\quad = \int_\Omega f(\boldsymbol{x}) u^{\mathfrak{M}}(\boldsymbol{x})\, d\boldsymbol{x} - R_\Gamma, \end{aligned} \tag{2.22}$$

where B_σ *is short for* $B_\sigma\left(\frac{b_{\mathrm{K}\sigma} d_\sigma}{\nu_\sigma}\right)$ *and* $R_\Gamma = \sum_{\sigma\in\boldsymbol{\mathcal{E}}_\Gamma} \left(F_{\mathrm{K},\sigma} - \frac{1}{2} b_{\mathrm{K}\sigma} u_\sigma\right) u_\sigma$.

Proof. Multiply (2.16) by u_K and sum over all the control volumes $\mathrm{K} \in \mathfrak{M}$ to obtain

$$\sum_{\mathrm{K}\in\mathfrak{M}} \left(\sum_{\sigma\in\boldsymbol{\mathcal{E}}_\mathrm{K}} F^d_{\mathrm{K},\sigma} u_\mathrm{K} + \sum_{\sigma\in\boldsymbol{\mathcal{E}}_\mathrm{K}} F^c_{\mathrm{K},\sigma} u_\mathrm{K} + |\mathrm{K}|\eta_\mathrm{K} u_\mathrm{K} u_\mathrm{K} \right) = \sum_{\mathrm{K}\in\mathfrak{M}} u_\mathrm{K} \int_\mathrm{K} f(\boldsymbol{x})\, d\boldsymbol{x}.$$

The two volume terms can be expressed as

$$\sum_{\mathrm{K}\in\mathfrak{M}} |\mathrm{K}|\eta_{\mathrm{K}}u_{\mathrm{K}}u_{\mathrm{K}} = \int_\Omega \eta(x)|u^{\mathfrak{M}}(\boldsymbol{x})|^2\,d\boldsymbol{x}, \qquad \sum_{\mathrm{K}\in\mathfrak{M}} u_{\mathrm{K}}\int_{\mathrm{K}} f(\boldsymbol{x})\,d\boldsymbol{x} = \int_\Omega f(\boldsymbol{x})u^{\mathfrak{M}}(\boldsymbol{x})\,d\boldsymbol{x}.$$

Let us now consider the diffusive terms

$$\begin{aligned}\sum_{\mathrm{K}\in\mathfrak{M}}\sum_{\sigma\in\boldsymbol{\mathcal{E}}_{\mathrm{K}}} F^d_{\mathrm{K},\sigma}u_{\mathrm{K}} &= \sum_{\sigma=\mathrm{K}\cap\mathrm{L}\in\boldsymbol{\mathcal{E}}_{int}} F^d_{\mathrm{K},\sigma}(u_{\mathrm{K}}-u_{\mathrm{L}}) + \sum_{\sigma\in\boldsymbol{\mathcal{E}}_D} F^d_{\mathrm{K},\sigma}u_{\mathrm{K}}\\ &\quad + \sum_{\sigma\in\boldsymbol{\mathcal{E}}_\Gamma} F^d_{\mathrm{K},\sigma}(u_{\mathrm{K}}-u_\sigma) + \sum_{\sigma\in\boldsymbol{\mathcal{E}}_\Gamma} F^d_{\mathrm{K},\sigma}u_\sigma\\ &= \sum_{\sigma\in\boldsymbol{\mathcal{E}}} \frac{|\sigma|\nu_\sigma}{d_\sigma}|u_{\mathrm{K}}-\tilde{u}_\sigma|^2 + \sum_{\sigma\in\boldsymbol{\mathcal{E}}_\Gamma} F^d_{\mathrm{K},\sigma}u_\sigma.\end{aligned}$$

The convective terms are treated in the same way:

$$\begin{aligned}\sum_{\mathrm{K}\in\mathfrak{M}}\sum_{\sigma\in\boldsymbol{\mathcal{E}}_{\mathrm{K}}} F^c_{\mathrm{K},\sigma}u_{\mathrm{K}} &= \sum_{\sigma=\mathrm{K}\cap\mathrm{L}\in\boldsymbol{\mathcal{E}}_{int}} F^c_{\mathrm{K},\sigma}(u_{\mathrm{K}}-u_{\mathrm{L}}) + \sum_{\sigma\in\boldsymbol{\mathcal{E}}_D} F^c_{\mathrm{K},\sigma}u_{\mathrm{K}}\\ &\quad + \sum_{\sigma\in\boldsymbol{\mathcal{E}}_\Gamma} F^c_{\mathrm{K},\sigma}(u_{\mathrm{K}}-u_\sigma) + \sum_{\sigma\in\boldsymbol{\mathcal{E}}_\Gamma} F^c_{\mathrm{K},\sigma}u_\sigma\\ &= \sum_{\sigma\in\boldsymbol{\mathcal{E}}} F^c_{\mathrm{K},\sigma}(u_{\mathrm{K}}-\tilde{u}_\sigma) + \sum_{\sigma\in\boldsymbol{\mathcal{E}}_\Gamma} F^c_{\mathrm{K},\sigma}u_\sigma.\end{aligned}$$

Then compute

$$\begin{aligned}\sum_{\sigma\in\boldsymbol{\mathcal{E}}} F^c_{\mathrm{K},\sigma}(u_{\mathrm{K}}-\tilde{u}_\sigma) &= \frac{1}{2}\sum_{\sigma\in\boldsymbol{\mathcal{E}}}|\sigma|b_{\mathrm{K}\sigma}(|u_{\mathrm{K}}|^2-|\tilde{u}_\sigma|^2) + \sum_{\sigma\in\boldsymbol{\mathcal{E}}}\frac{|\sigma|\nu_\sigma}{d_\sigma}B_\sigma|u_{\mathrm{K}}-\tilde{u}_\sigma|^2\\ &= \frac{1}{2}\sum_{\mathrm{K}\in\mathfrak{M}}\left(\sum_{\sigma\in\boldsymbol{\mathcal{E}}_{\mathrm{K}}}|\sigma|b_{\mathrm{K}\sigma}\right)|u_{\mathrm{K}}|^2 - \frac{1}{2}\sum_{\sigma\in\boldsymbol{\mathcal{E}}_\Gamma}|\sigma|b_{\mathrm{K}\sigma}|u_\sigma|^2\\ &\quad + \sum_{\sigma\in\boldsymbol{\mathcal{E}}}\frac{|\sigma|\nu_\sigma}{d_\sigma}B_\sigma|u_{\mathrm{K}}-\tilde{u}_\sigma|^2\\ &= \frac{1}{2}\int_\Omega(\mathrm{div}\mathbf{b})\,|u^{\mathfrak{M}}(\boldsymbol{x})|^2\,d\boldsymbol{x} - \frac{1}{2}\sum_{\sigma\in\boldsymbol{\mathcal{E}}_\Gamma}|\sigma|b_{\mathrm{K}\sigma}|u_\sigma|^2\\ &\quad + \sum_{\sigma\in\boldsymbol{\mathcal{E}}}\frac{|\sigma|\nu_\sigma}{d_\sigma}B_\sigma|u_{\mathrm{K}}-\tilde{u}_\sigma|^2.\end{aligned}$$

Gathering all terms yields (2.22). ∎

LEMMA 2.4. *The discrete boundary operator* Λ_Γ *in* (2.15) *has the following properties:*

1. *It is a symmetric positive definite operator, satifying if* $\nu(v)\geq\bar{\nu}>0$ *a.e. in* Ω*,*

$$(\Lambda_\Gamma\mathbf{u}^{\boldsymbol{\mathcal{E}}_\Gamma},\mathbf{u}^{\boldsymbol{\mathcal{E}}_\Gamma}) \geq p\|\mathbf{u}^{\boldsymbol{\mathcal{E}}_\Gamma}\|^2_{0,\Gamma} + q\bar{\nu}\|\mathbf{u}^{\boldsymbol{\mathcal{E}}_\Gamma}\|^2_{1,\boldsymbol{\mathcal{E}}_\Gamma}.$$

2. *If* $\mathbf{u}^{\mathcal{T}} = (\mathbf{u}^{\mathfrak{M}},\mathbf{u}^{\boldsymbol{\mathcal{E}}_\Gamma})$ *solves* (2.16, 2.17)*, then*

$$(\Lambda_\Gamma\mathbf{u}^{\boldsymbol{\mathcal{E}}_\Gamma},\mathbf{u}^{\boldsymbol{\mathcal{E}}_\Gamma}) = R_\Gamma + \int_\Gamma u^{\boldsymbol{\mathcal{E}}_\Gamma}(y)\,g(y)\,dy. \tag{2.23}$$

Proof. Compute

$$(\Lambda_\Gamma \mathbf{u}^{\boldsymbol{\mathcal{E}}_\Gamma}, \mathbf{u}^{\boldsymbol{\mathcal{E}}_\Gamma}) = p\sum_{i=1}^{|\boldsymbol{\mathcal{E}}_\Gamma|} |\sigma_i||u_{\sigma_i}|^2 + q\sum_{i=1}^{|\boldsymbol{\mathcal{E}}_\Gamma|}(F_{i+\frac12} - F_{i-\frac12})u_{\sigma_i}$$

$$= p\sum_{i=1}^{|\boldsymbol{\mathcal{E}}_\Gamma|} |\sigma_i||u_{\sigma_i}|^2 + q\sum_{i=0}^{|\boldsymbol{\mathcal{E}}_\Gamma|} F_{i+\frac12}(u_{\sigma_i} - u_{\sigma_{i+1}})$$

$$\geqslant p\|\mathbf{u}^{\boldsymbol{\mathcal{E}}_\Gamma}\|_{0,\Gamma}^2 + q\bar\nu\|\mathbf{u}^{\boldsymbol{\mathcal{E}}_\Gamma}\|_{1,\boldsymbol{\mathcal{E}}_\Gamma}^2.$$

Now multiply (2.17) by u_{σ_i} and sum over the edges of Γ to obtain

$$\sum_{i=1}^{|\boldsymbol{\mathcal{E}}_\Gamma|}\left(-F_{\mathrm{K}_i,\sigma_i} + \frac12|\sigma_i|b_{\mathrm{K}_i\sigma_i}u_{\sigma_i}\right)u_{\sigma_i} + (\Lambda_\Gamma \mathbf{u}^{\boldsymbol{\mathcal{E}}_\Gamma}, \mathbf{u}^{\boldsymbol{\mathcal{E}}_\Gamma}) = \sum_{i=1}^{|\boldsymbol{\mathcal{E}}_\Gamma|} u_{\sigma_i}\int_{\sigma_i} g(y)\,dy.$$

Estimate (2.23) follows immediately from the definition of R_Γ in Lemma 2.3. ∎

PROPOSITION 2.5 (A priori estimates). *Let $f \in L^2(\Omega)$, $g \in L^2(\Gamma)$, $\nu \in W^{1,\infty}(\Omega)$ such that $\nu(x) \geq \bar\nu > 0$ a.e. $x \in \Omega$. Assume furthermore that for all $\sigma \in \boldsymbol{\mathcal{E}}$, B_σ satisfies* (2.11)*, $p > 0$, $q \geq 0$. Then there exists a positive number C such that for any $\mathbf{u}^{\mathcal{T}} = (\mathbf{u}^{\mathfrak{M}}, \mathbf{u}^{\boldsymbol{\mathcal{E}}_\Gamma})$ solution of* (2.16), (2.17)*, the following estimate holds:*

$$\|\mathbf{u}^{\mathcal{T}}\|_{1,\mathcal{T}}^2 + p\|\mathbf{u}^{\boldsymbol{\mathcal{E}}_\Gamma}\|_{0,\Gamma}^2 + q\|\mathbf{u}^{\boldsymbol{\mathcal{E}}_\Gamma}\|_{1,\boldsymbol{\mathcal{E}}_\Gamma}^2 \leq C\left(\|f\|_{0,\Omega}^2 + \|g\|_{0,\Gamma}^2\right). \tag{2.24}$$

Proof. This is a consequence of Lemmas 2.3 and 2.4 and Poincaré inequalities (2.21). ∎

The a priori estimate yields uniqueness of the solution of the discrete equations. Well-posedness follows immediately.

COROLLARY 2.6. *Let $f \in L^2(\Omega)$, $g \in L^2(\Gamma)$, $\nu \in W^{1,\infty}(\Omega)$ such that $\nu(x) \geq \bar\nu > 0$ for all x in Ω. Assume that $(B_\sigma)_{\sigma\in\boldsymbol{\mathcal{E}}}$ satisfies* (2.11)*, $p > 0$, $q \geq 0$. Then* (2.16), (2.17) *admit a unique solution.*

2.7. Error estimates. For $u \in \mathcal{W}_m(\Omega)$, define for all control volumes $\bar u_{\mathrm{K}} = u(\boldsymbol{x}_{\mathrm{K}})$ and all edges $\bar u_\sigma = u(\boldsymbol{x}_\sigma)$; then $\bar{\mathbf{u}}^{\mathfrak{M}} = (\bar u_{\mathrm{K}})_{\mathrm{K}\in\mathfrak{M}}$, $\bar{\mathbf{u}}^{\boldsymbol{\mathcal{E}}_\Gamma} = (\bar u_\sigma)_{\sigma\in\boldsymbol{\mathcal{E}}_\Gamma}$, $\bar{\mathbf{u}}^{\mathcal{T}} = (\bar{\mathbf{u}}^{\mathfrak{M}}, \bar{\mathbf{u}}^{\boldsymbol{\mathcal{E}}_\Gamma})$. The aim of this section is to prove the following error estimates.

THEOREM 2.7. *There exists a positive constant C such that for any $u \in \mathcal{W}_m(\Omega)$, the solution of problem* (2.1)*, and $\mathbf{u}^{\mathcal{T}} = (\mathbf{u}^{\mathfrak{M}}, \mathbf{u}^{\boldsymbol{\mathcal{E}}_\Gamma})$, the solution of the discrete counterpart* (2.16), (2.17)*, we have*

$$\|\bar{\mathbf{u}}^{\mathcal{T}} - \mathbf{u}^{\mathcal{T}}\|_{1,\mathcal{T}}^2 + p\|\bar{\mathbf{u}}^{\boldsymbol{\mathcal{E}}_\Gamma} - \mathbf{u}^{\boldsymbol{\mathcal{E}}_\Gamma}\|_{0,\Gamma}^2 + q\|\bar{\mathbf{u}}^{\boldsymbol{\mathcal{E}}_\Gamma} - \mathbf{u}^{\boldsymbol{\mathcal{E}}_\Gamma}\|_{1,\boldsymbol{\mathcal{E}}_\Gamma}^2 \leq C(\mathrm{reg}(\mathcal{T}))\mathrm{size}(\mathfrak{M})^2\|u\|_{\mathcal{W}_m(\Omega)}^2.$$

The proof of this theorem follows classical lines, starting with consistency errors.

2.7.1. Consistency errors. Integrate (1.1) over the control volume $\mathrm{K} \in \mathfrak{M}$:

$$-\sum_{\sigma\in\boldsymbol{\mathcal{E}}_{\mathrm{K}}}\int_\sigma \nu\nabla u\cdot n_{\mathrm{K},\sigma}\,ds + \int_\sigma \mathbf{b}\cdot\mathbf{n}_{\mathrm{K}\sigma}u\,ds + \int_{\mathrm{K}}\eta u\,d\boldsymbol{x} = \int_{\mathrm{K}} f(\boldsymbol{x})\,d\boldsymbol{x}. \tag{2.25}$$

For $\mathrm{K} \in \mathfrak{M}$ and $\sigma \in \boldsymbol{\mathcal{E}}_{\mathrm{K}}$, introduce the discrete diffusive and convective fluxes associated to the exact solution,

$$\overline{F_{\mathrm{K},\sigma}^d} = |\sigma|\nu_\sigma\frac{\bar u_{\mathrm{K}} - \widetilde{\bar u}_\sigma}{d_\sigma}, \quad \overline{F_{\mathrm{K},\sigma}^c} = \frac12|\sigma|b_{\mathrm{K}\sigma}(\bar u_{\mathrm{K}} + \widetilde{\bar u}_\sigma) + \frac{|\sigma|\nu_\sigma}{d_\sigma}B_\sigma\left(\frac{d_\sigma b_{\mathrm{K}\sigma}}{\nu_\sigma}\right)(\bar u_{\mathrm{K}} - \widetilde{\bar u}_\sigma),$$

with $\widetilde{\overline{u}}_\sigma$ defined as in (2.14), by

$$\widetilde{\overline{u}}_\sigma = \begin{cases} \bar{u}_{\mathrm{L}} & \text{if } \sigma \in \boldsymbol{\mathcal{E}}_{int}, \\ 0 & \text{if } \sigma \in \boldsymbol{\mathcal{E}}_D, \\ \bar{u}_\sigma & \text{if } \sigma \in \boldsymbol{\mathcal{E}}_\Gamma. \end{cases}$$

Define the consistency error of the diffusive and convective fluxes and of the volume term by

$$R^d_{\mathrm{K},\sigma} = \overline{F^d_{\mathrm{K},\sigma}} + \int_\sigma \nu \nabla u \cdot n_{\mathrm{K},\sigma}\, ds,$$
$$R^c_{\mathrm{K},\sigma} = \overline{F^c_{\mathrm{K},\sigma}} - \int_\sigma (\mathbf{b}\cdot \mathbf{n}_{\mathrm{K}\sigma}) u\, ds,$$
$$R^v_{\mathrm{K}} = \int_{\mathrm{K}} \eta(u - \bar{u}_{\mathrm{K}})\, d\boldsymbol{x}.$$

Equation (2.25) can be rewritten as

$$\sum_{\sigma\in\boldsymbol{\mathcal{E}}_{\mathrm{K}}} \left(\overline{F^d_{\mathrm{K},\sigma}} + \overline{F^c_{\mathrm{K},\sigma}}\right) + |\mathrm{K}|\eta_{\mathrm{K}}\bar{u}_{\mathrm{K}} = \sum_{\sigma\in\boldsymbol{\mathcal{E}}_{\mathrm{K}}} (R^d_{\mathrm{K},\sigma} + R^c_{\mathrm{K},\sigma}) + R^v_{\mathrm{K}} + \int_{\mathrm{K}} f(\boldsymbol{x})\, d\boldsymbol{x}.$$

Subtracting the corresponding discrete equation (2.16) yields

$$\sum_{\sigma\in\boldsymbol{\mathcal{E}}_{\mathrm{K}}} (\overline{F^d_{\mathrm{K},\sigma}} - F^d_{\mathrm{K},\sigma}) + \sum_{\sigma\in\boldsymbol{\mathcal{E}}_{\mathrm{K}}} (\overline{F^c_{\mathrm{K},\sigma}} - F^c_{\mathrm{K},\sigma}) + \sum_{\mathrm{K}\in\mathfrak{M}} \eta(\bar{u}_{\mathrm{K}} - u_{\mathrm{K}}) = \bar{f}^{\mathcal{T}}_{\mathrm{K}} \tag{2.26}$$

with

$$\bar{f}^{\mathcal{T}}_{\mathrm{K}} := \sum_{\sigma\in\boldsymbol{\mathcal{E}}_{\mathrm{K}}} (R^d_{\mathrm{K},\sigma} + R^c_{\mathrm{K},\sigma}) + R^v_{\mathrm{K}}. \tag{2.27}$$

Now integrate the boundary condition (2.1c) over each edge $\sigma_i \in \boldsymbol{\mathcal{E}}_\Gamma$:

$$\int_{\sigma_i} \nu\nabla u\cdot \mathbf{n}_{\mathrm{K}_i\sigma_i}\, dy - \frac{1}{2}\int_{\sigma_i} (\mathbf{b}\cdot\mathbf{n}_{\mathrm{K}_i\sigma_i}) u\, dy + \int_{\sigma_i} pu\, dy + q\,[-\nu\nabla u\cdot\tau]^{\boldsymbol{x}_{i+\frac12}}_{\boldsymbol{x}_{i-\frac12}} = \int_{\sigma_i} g\, dy.$$

Introduce the one-dimensional diffusion consistency error

$$r_{i+\frac12} = \overline{F_{i+\frac12}} + \nu(\boldsymbol{x}_{i+\frac12})(\nabla u\cdot\tau)(\boldsymbol{x}_{i+\frac12}), \text{ where } \overline{F_{i+\frac12}} = \nu(\boldsymbol{x}_{i+\frac12})\frac{u(\boldsymbol{x}_i) - u(\boldsymbol{x}_{i+1})}{d_{i+\frac12}}$$

and the one-dimensional volume consistency error

$$r_\sigma = \int_\sigma \left(p + \frac{1}{2}\mathbf{b}\cdot\mathbf{n}\right) u(\boldsymbol{x}_\sigma)\, dy - \int_\sigma \left(p + \frac{1}{2}\frac{1}{|\sigma|}\int_\sigma \mathbf{b}\cdot\mathbf{n}\right) u(\boldsymbol{x}_\sigma)\, dy,$$

where $\mathbf{n}$ stands for the outward unit normal to Γ. Subtracting the discrete equation (2.17) yields

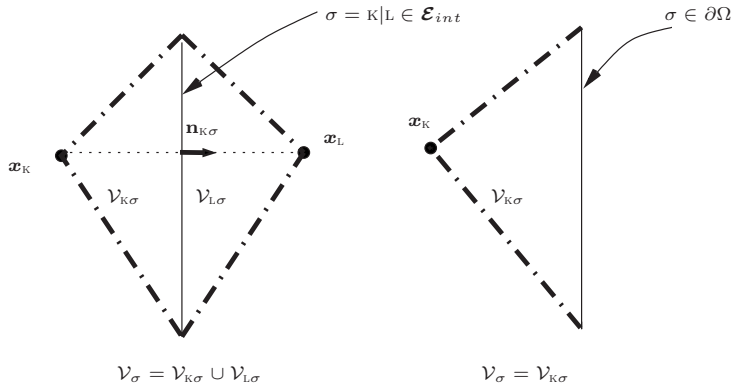

FIG. 4. *The diamond cells.*

$$
\begin{aligned}
(2.28)\qquad & -(\overline{F^d_{\mathrm{K}i,\sigma_i}} - F^d_{\mathrm{K}i,\sigma_i}) - (\overline{F^c_{\mathrm{K}i,\sigma_i}} - F^c_{\mathrm{K}i,\sigma_i}) + \left(p + \frac{1}{2} b_{\mathrm{K}i\sigma_i}\right) |\sigma_i| e_{\sigma_i} \\
& + q((\overline{F_{i+\frac{1}{2}}} - F_{i+\frac{1}{2}}) - (\overline{F_{i-\frac{1}{2}}} - F_{i-\frac{1}{2}})) = \overline{g}_i^{\mathcal{T}}
\end{aligned}
$$

with

$$
(2.29)\qquad \overline{g}_i^{\mathcal{T}} := -R^d_{\mathrm{K},\sigma_i} - R^c_{\mathrm{K},\sigma_i} - r_{\sigma_i} + q(r_{i+\frac{1}{2}} - r_{i-\frac{1}{2}}).
$$

The next task is to estimate the consistency errors. This will be done using the diamond cells defined in Figure 4.

LEMMA 2.8. *Assume that* $\mathbf{b} \in W^{1,\infty}(\Omega)$, $\nu \in W^{1,\infty}(\Omega)$, $\eta \in L^\infty(\Omega)$. *Then for any* $\alpha > 2$, *there exists a real number* $C > 0$ *such that for any* $u \in \mathcal{W}_m(\Omega)$, *the consistency errors can be estimated by*

$$
\begin{aligned}
\frac{d_\sigma}{|\sigma|} |R^d_{\mathrm{K},\sigma}|^2 &\leqslant C\ \mathrm{size}(\mathfrak{M})^2 \int_{\mathcal{V}_\sigma} |D^2 u(\boldsymbol{x})|^2\, d\boldsymbol{x}\ \forall \mathrm{K} \in \mathfrak{M},\ \sigma \in \boldsymbol{\mathcal{E}}_{\mathrm{K}}, \\
\frac{d_\sigma}{|\sigma|} |R^c_{\mathrm{K},\sigma}|^2 &\leqslant C\ \mathrm{size}(\mathfrak{M})^2 |\mathcal{V}_\sigma|^{1-\frac{2}{\alpha}} \left(\int_{\mathcal{V}_\sigma} |\nabla u(\boldsymbol{x})|^\alpha\, d\boldsymbol{x} \right)^{\frac{2}{\alpha}}\ \forall \mathrm{K} \in \mathfrak{M},\ \sigma \in \boldsymbol{\mathcal{E}}_{\mathrm{K}}, \\
\frac{1}{|\mathrm{K}|} |R^v_{\mathrm{K}}|^2 &\leqslant C\ \mathrm{size}(\mathfrak{M})^2 |\mathrm{K}|^{1-\frac{2}{\alpha}} \left(\int_{\mathrm{K}} |\nabla u(\boldsymbol{x})|^\alpha\, d\boldsymbol{x} \right)^{\frac{2}{\alpha}}\ \forall \mathrm{K} \in \mathfrak{M}, \\
\frac{d_{i+\frac{1}{2}}}{|\sigma_i|} |r_{i+\frac{1}{2}}|^2 &\leqslant C\ \mathrm{size}(\mathfrak{M})^2 \int_{\boldsymbol{x}_i}^{\boldsymbol{x}_{i+1}} |\partial_{yy} u|^2\, dy \text{ for } i = 0, \ldots, |\boldsymbol{\mathcal{E}}_\Gamma|, \\
\frac{1}{|\sigma|} |r_\sigma|^2 &\leqslant C\ \mathrm{size}(\mathfrak{M})^2 |\sigma|^{1-\frac{2}{\alpha}} \left(\int_\sigma |\partial_y u|^\alpha\, dy \right)^{\frac{2}{\alpha}} \text{ for } \sigma \in \boldsymbol{\mathcal{E}}_\Gamma.
\end{aligned}
$$

Proof. The proof of this technical lemma is classical and can be found, e.g., in [10, 12]. ∎

2.7.2. End of the proof of Theorem 2.7. Define the error with the same notation as before by $e_{\mathrm{K}} = \bar{u}_{\mathrm{K}} - u_{\mathrm{K}}$ and $e_\sigma = \bar{u}_\sigma - u_\sigma$. By linearity, Lemmas 2.3 and 2.4 apply to $\mathbf{e}^{\mathcal{T}}$, with right-hand sides given by the families of $\bar{f}^{\mathcal{T}}_{\mathrm{K}}$ in (2.27) and $\overline{g}^{\mathcal{T}}_i$ in (2.29). Introduce $\widetilde{e}_\sigma = \widetilde{\overline{u}}_\sigma - \widetilde{u}_\sigma$, and use the previous lemmas to estimate

$$\begin{aligned}\sum_{\kappa\in\mathfrak{M}} e_{\kappa}\bar{f}_{\kappa}^{\mathcal{T}} &= \sum_{\kappa\in\mathfrak{M}} e_{\kappa}\left(\sum_{\sigma\in\boldsymbol{\mathcal{E}}_{\kappa}}(R^d_{\kappa,\sigma}+R^c_{\kappa,\sigma})+R^v_{\kappa}\right)\\ &= \sum_{\sigma\in\boldsymbol{\mathcal{E}}}(R^d_{\kappa,\sigma}+R^c_{\kappa,\sigma})(e_{\kappa}-\widetilde{e}_{\sigma})+\sum_{\sigma\in\boldsymbol{\mathcal{E}}_{\Gamma}}(R^d_{\kappa,\sigma}+R^c_{\kappa,\sigma})e_{\sigma}+\sum_{\kappa\in\mathfrak{M}} e_{\kappa}R^v_{\kappa}\\ &\leqslant \|\mathbf{e}^{\mathcal{T}}\|_{1,\mathcal{T}}\left(\sum_{\sigma\in\boldsymbol{\mathcal{E}}}\frac{d_{\sigma}}{|\sigma|}\,|R^d_{\kappa,\sigma}+R^c_{\kappa,\sigma}|^2\right)^{\frac12}+\sum_{\sigma\in\boldsymbol{\mathcal{E}}_{\Gamma}}(R^d_{\kappa,\sigma}+R^c_{\kappa,\sigma})e_{\sigma}\\ &\quad+\|\mathbf{e}^{\mathfrak{M}}\|_{0,\Omega}\left(\sum_{\kappa\in\mathfrak{M}}\frac{1}{|\mathrm{K}|}|R^v_{\kappa}|^2\right)^{\frac12}.\end{aligned}$$

In the same way,

$$\begin{aligned}\sum_{i=1}^{|\boldsymbol{\mathcal{E}}_{\Gamma}|} e_{\sigma_i}\overline{g}_i^{\mathcal{T}} &= \sum_{i=1}^{|\boldsymbol{\mathcal{E}}_{\Gamma}|} e_{\sigma_i}\left(-R^d_{\kappa,\sigma_i}-R^c_{\kappa,\sigma_i}-r_{\sigma_i}+q(r_{i+\frac12}-r_{i-\frac12})\right)\\ &= \sum_{i=1}^{|\boldsymbol{\mathcal{E}}_{\Gamma}|} e_{\sigma_i}\left(-R^d_{\kappa,\sigma_i}-R^c_{\kappa,\sigma_i}-r_{\sigma_i}\right)+q\sum_{i=0}^{|\boldsymbol{\mathcal{E}}_{\Gamma}|} r_{i+\frac12}(e_{\sigma_i}-e_{\sigma_{i+1}})\\ &\leqslant \sum_{i=1}^{|\boldsymbol{\mathcal{E}}_{\Gamma}|} e_{\sigma_i}\left(-R^d_{\kappa,\sigma_i}-R^c_{\kappa,\sigma_i}\right)+\|\mathbf{e}^{\boldsymbol{\mathcal{E}}_{\Gamma}}\|_{0,\Gamma}\left(\sum_{\sigma\in\Gamma}\frac{1}{|\sigma|}|r_{\sigma}|^2\right)^{\frac12}\\ &\quad+q\|\mathbf{e}^{\boldsymbol{\mathcal{E}}_{\Gamma}}\|_{1,\boldsymbol{\mathcal{E}}_{\Gamma}}\left(\sum_{i=0}^{|\boldsymbol{\mathcal{E}}_{\Gamma}|}\frac{d_{i+\frac12}}{|\sigma_i|}|r_{i+\frac12}|^2\right)^{\frac12}.\end{aligned}$$

Summing the last two inequalities yields

$$\begin{aligned}\sum_{\kappa\in\mathfrak{M}} e_{\kappa}\bar{f}_{\kappa}^{\mathcal{T}}+\sum_{i=1}^{|\boldsymbol{\mathcal{E}}_{\Gamma}|} e_{\sigma_i}\overline{g}^{\mathcal{T}} &\leqslant \|\mathbf{e}^{\mathcal{T}}\|_{1,\mathcal{T}}\left(\sum_{\sigma\in\boldsymbol{\mathcal{E}}}\frac{d_{\sigma}}{|\sigma|}\,|R^d_{\kappa,\sigma}+R^c_{\kappa,\sigma}|^2\right)^{\frac12}\\ &\quad+\|\mathbf{e}^{\mathfrak{M}}\|_{0,\Omega}\left(\sum_{\kappa\in\mathfrak{M}}\frac{1}{|\mathrm{K}|}|R^v_{\kappa}|^2\right)^{\frac12}+\|\mathbf{e}^{\boldsymbol{\mathcal{E}}_{\Gamma}}\|_{0,\Gamma}\left(\sum_{\sigma\in\boldsymbol{\mathcal{E}}_{\Gamma}}\frac{1}{|\sigma|}|r_{\sigma}|^2\right)^{\frac12}\\ &\quad+q\|\mathbf{e}^{\boldsymbol{\mathcal{E}}_{\Gamma}}\|_{1,\boldsymbol{\mathcal{E}}_{\Gamma}}\left(\sum_{i=0}^{|\boldsymbol{\mathcal{E}}_{\Gamma}|}\frac{d_{i+\frac12}}{|\sigma|}|r_{i+\frac12}|^2\right)^{\frac12}.\end{aligned}$$

Young's inequality together with the discrete Poincaré inequality (2.21) lead to the new estimate

$$\begin{aligned}&\frac{1}{C}\left(\|\mathbf{e}^{\mathcal{T}}\|^2_{1,\mathcal{T}}+\|\mathbf{e}^{\mathfrak{M}}\|^2_{L^2(\Omega)}+p\|\mathbf{e}^{\boldsymbol{\mathcal{E}}_{\Gamma}}\|^2_{0,\Gamma}+q\|\mathbf{e}^{\boldsymbol{\mathcal{E}}_{\Gamma}}\|^2_{1,\boldsymbol{\mathcal{E}}_{\Gamma}}\right)\\ &\quad\leqslant\sum_{\sigma\in\boldsymbol{\mathcal{E}}}\frac{d_{\sigma}}{|\sigma|}\,|R^d_{\kappa,\sigma}+R^c_{\kappa,\sigma}|^2+\sum_{\kappa\in\mathfrak{M}}\frac{1}{|\mathrm{K}|}|R^v_{\kappa}|^2+p\sum_{\sigma\in\boldsymbol{\mathcal{E}}_{\Gamma}}\frac{1}{|\sigma|}|r_{\sigma}|^2+q\sum_{i=0}^{|\boldsymbol{\mathcal{E}}_{\Gamma}|}\frac{d_{i+\frac12}}{|\sigma_i|}|r_{i+\frac12}|^2.\end{aligned}$$

Lemma 2.8 and Sobolev embeddings conclude the proof of Theorem 2.7.

3. A Schwarz algorithm with Ventcell transmission conditions. The aim of this section is to design and study a discrete version of the Ventcell–Schwarz algorithm, designed by using an elliptic boundary operator Λ, defined by $\Lambda\phi = p\phi - q\partial_y(\nu\partial_y\phi)$. For $j \in (1,2)$, the algorithm computes u_j^n using boundary data at step $n-1$ coming from the neighboring subdomain Ω_i. An appropriate initial guess is given:

$$\mathcal{L}u_j^n = f \text{ on } \Omega_j, \tag{3.1a}$$

$$\left(\nu\partial_{n_j} - \frac{1}{2}\mathbf{b}\cdot\mathbf{n}_j + \Lambda\right)u_j^n = \left(-\nu_i\partial_{n_i} + \frac{1}{2}\mathbf{b}\cdot\mathbf{n}_i + \Lambda\right)u_i^{n-1} \text{ on } \Gamma. \tag{3.1b}$$

3.1. Convergence at the continuous level.

THEOREM 3.1. *For any initial guess (u_1^0, u_2^0) in $\mathcal{W}_m(\Omega_1)\times\mathcal{W}_m(\Omega_2)$, (3.1) defines a sequence of iterates in $\mathcal{W}_m(\Omega_1)\times\mathcal{W}_m(\Omega_2)$, which converges in $H^1(\Omega_1)\times H^1(\Omega_2)$ to the solution u of (1.1).*

Proof. First identify u as the potential limit of (3.1). By linearity, only the convergence to zero of the sequences of iterates with $f = 0$ has to be proved. Defining the continuous flux $F_j^n = -(\nu\partial_{n_j} - \frac{1}{2}\mathbf{b}\cdot\mathbf{n}_j)u_j^n$, the transmission condition on Γ takes the form

$$-F_j^n + \Lambda u_j^n = F_i^{n-1} + \Lambda u_i^{n-1}. \tag{3.2}$$

Multiplying (3.1a) by u_j^n yields

$$a_{\Omega_j}(u_j^n, u_j^n) + R^{n,j} = 0, \quad R^{n,j} = \langle F_j^n, u_j^n\rangle_\Gamma. \tag{3.3}$$

The boundary term $R^{n,j}$ can be rewritten using the scalar product defined by Λ^{-1} in (2.4):

$$R^{n,j} = \langle F_j^n, \Lambda^{-1}\Lambda u_j^n\rangle_\Gamma = \langle F_j^n, \Lambda u_j^n\rangle_{\Lambda^{-1}} = \frac{1}{4}\|F_j^n + \Lambda u_j^n\|_{\Lambda^{-1}}^2 - \frac{1}{4}\|F_j^n - \Lambda u_j^n\|_{\Lambda^{-1}}^2.$$

Plug this last expression into (3.3) to obtain

$$a_{\Omega_j}(u_j^n, u_j^n) + \frac{1}{4}\|F_j^n + \Lambda u_j^n\|_{\Lambda^{-1}}^2 = \frac{1}{4}\|F_j^n - \Lambda u_j^n\|_{\Lambda^{-1}}^2.$$

Replace the right-hand side using the transmission condition (3.2) to get

$$a_{\Omega_j}(u_j^n, u_j^n) + \frac{1}{4}\|F_j^n + \Lambda u_j^n\|_{\Lambda^{-1}}^2 = \frac{1}{4}\|F_i^{n-1} + \Lambda u_i^{n-1}\|_{\Lambda^{-1}}^2.$$

Sum the previous equalities over the subdomains and the iterations to obtain for each $N \geq 1$,

$$\sum_{n=1}^{N}\sum_{j=1}^{2} a_{\Omega_j}(u_j^n, u_j^n) + \frac{1}{4}\sum_{j=1}^{2}\|F_j^N + \Lambda u_j^N\|_{\Lambda^{-1}}^2 = \frac{1}{4}\sum_{j=1}^{2}\|F_j^0 + \Lambda u_j^0\|_{\Lambda^{-1}}^2.$$

This last equality proves that u_j^n tends to zero in $H^1(\Omega_j)$. ∎

3.2. Discrete Schwarz algorithm. Given a composite mesh $\mathcal{T} = (\mathfrak{M}, \mathfrak{M}_1, \mathfrak{M}_2, \boldsymbol{\mathcal{E}}_\Gamma)$, the discrete Schwarz algorithm consists, with suitable initial data, in finding for all $n \geq 1$ the solutions $\mathbf{u}^{\mathcal{T}_j,n} = (\mathbf{u}^{\mathfrak{M}_j,n}, \mathbf{u}^{\boldsymbol{\mathcal{E}}_\Gamma^j,n})$ of the linear system

$$\forall \mathrm{K} \in \mathfrak{M}_j, \quad \sum_{\sigma \in \boldsymbol{\mathcal{E}}_\mathrm{K}} (F_{\mathrm{K},\sigma})_j^n + |\mathrm{K}| \eta_\mathrm{K}(u_\mathrm{K})_j^n = \int_\mathrm{K} f(\boldsymbol{x})\, d\boldsymbol{x}, \tag{3.4a}$$

$$\forall \sigma \in \boldsymbol{\mathcal{E}}_\Gamma, \quad \begin{aligned} &-(F_{\mathrm{K},\sigma})_j^n + \frac{1}{2}\mathbf{b}\cdot n_j |\sigma| (u_\sigma)_j^n + \Lambda_\Gamma(u_\sigma)_j^n \\ &\quad = (F_{\mathrm{K},\sigma})_i^{n-1} - \frac{1}{2}\mathbf{b}\cdot \mathbf{n}_i |\sigma| (u_\sigma)_i^{n-1} + \Lambda_\Gamma(u_\sigma)_i^{n-1}. \end{aligned} \tag{3.4b}$$

The notation introduced in section 2 naturally extends here. For $j = 1, 2$, the discrete boundary operators Λ_Γ^j and Λ_Γ^i coincide, and the common value Λ_Γ is given by

$$\forall \sigma = \sigma_l \in \boldsymbol{\mathcal{E}}_\Gamma,\ \Lambda_\Gamma(u_\sigma)_j = p|\sigma|(u_\sigma)_j - q((F_{l+\frac{1}{2}})_j - (F_{l-\frac{1}{2}})_j). \tag{3.5}$$

Note that since $(F_{\mathrm{K},\sigma})_j^n$ approximates the flux $(-\nu\partial_{n_j} + \mathbf{b}\cdot\mathbf{n}_j)(u_j^n)$, the term in (3.4b), $-(F_{\mathrm{K},\sigma})_j^n + \frac{1}{2}\mathbf{b}\cdot n_j|\sigma|(u_\sigma)_j^n$ is an approximation of $(\nu\partial_{n_j} - \frac{1}{2}\mathbf{b}\cdot\mathbf{n}_j)(u_j^n)$.

3.3. Convergence of the discrete Schwarz algorithm. Since the global mesh $\mathfrak{M}$ is the composition of the two local meshes, the first task will be to identify the limit of the sequence of finite volume problems in (3.4). It turns out that it still is a finite volume scheme on the composite mesh for problem (1.1), but with a modified convective flux $\widetilde{B}_\sigma$. This will be emphasized in Theorem 3.2, and convergence will be proved. Alternatively, given a finite volume discretization of problem (1.1) with a convective flux $\widetilde{B}_\sigma$, Theorem 3.3 will investigate under which conditions there exists a modified Schwarz algorithm converging to the solution of that scheme.

THEOREM 3.2. *Let $\mathcal{T}_j$ be two compatible meshes of Ω_j, $j = 1, 2$, and let $\mathcal{T}$ be the associated composite mesh. Let $\mathbf{u}^{\mathcal{T}_j,n} = (\mathbf{u}^{\mathfrak{M}_j,n}, \mathbf{u}^{\boldsymbol{\mathcal{E}}_\Gamma^j,n})$ be the solution of* (3.4) *with convective fluxes $(B_\sigma)_{\sigma\in\boldsymbol{\mathcal{E}}_\Gamma}$ in* (2.10) *satisfying* (2.11). *Then $(\mathbf{u}^{\mathfrak{M}_1,n}, \mathbf{u}^{\mathfrak{M}_2,n})$ converges to $\mathbf{u}^{\mathfrak{M}} = (\mathbf{u}^{\mathfrak{M}_1}, \mathbf{u}^{\mathfrak{M}_2})$, which is a discrete approximation of the solution u of problem* (1.1), *the solution of the following:*

$$\forall \mathrm{K} \in \mathfrak{M}, \quad \sum_{\sigma \in \boldsymbol{\mathcal{E}}_\mathrm{K}} F_{\mathrm{K},\sigma} + |\mathrm{K}|\eta_\mathrm{K} u_\mathrm{K} = \int_\mathrm{K} f(\boldsymbol{x})\, d\boldsymbol{x}, \tag{3.6}$$

where $F_{\mathrm{K},\sigma} = F_{\mathrm{K},\sigma}^d + F_{\mathrm{K},\sigma}^c$ is defined in (2.9), (2.10) *with a new appropriate choice $\widetilde{B}_\sigma$ of the convective flux on $\sigma \in \boldsymbol{\mathcal{E}}_\Gamma$, given by* (3.10).

Proof. First step: Identification of the limit. Assume that $\mathbf{u}^{\mathcal{T}_j,n}$ converges to $\mathbf{u}^{\mathcal{T}_j} = (\mathbf{u}^{\mathfrak{M}_j}, \mathbf{u}^{\boldsymbol{\mathcal{E}}_\Gamma^j})$ as n tends to infinity. We first prove that

$$\forall \mathrm{K} \in \mathfrak{M}_j, \quad \sum_{\sigma \in \boldsymbol{\mathcal{E}}_\mathrm{K}} (F_{\mathrm{K},\sigma})_j + |\mathrm{K}|\eta_\mathrm{K}(u_\mathrm{K})_j = \int_\mathrm{K} f(\boldsymbol{x})\, d\boldsymbol{x}, \tag{3.7a}$$

$$\forall \sigma \in \boldsymbol{\mathcal{E}}_\Gamma, \sigma = \partial\mathrm{K}_1 \cap \partial\mathrm{K}_2 \text{ with } \mathrm{K}_i \in \mathfrak{M}_i, \quad -(F_{\mathrm{K}_1,\sigma})_1 = (F_{\mathrm{K}_2,\sigma})_2. \tag{3.7b}$$

Passing to the limit in system (3.4) yields (3.7a), and for $(j, i) = (1, 2)$ and $(2, 1)$

$$-(F_{\mathrm{K}_j,\sigma})_j + \frac{1}{2}\mathbf{b}\cdot n_j|\sigma|(u_\sigma)_j + \Lambda_\Gamma(u_\sigma)_j = (F_{\mathrm{K}_i,\sigma})_i - \frac{1}{2}\mathbf{b}\cdot\mathbf{n}_i|\sigma|(u_\sigma)_i + \Lambda_\Gamma(u_\sigma)_i. \tag{3.8}$$

Adding (3.8) in $(1, 2)$ and $(2, 1)$ gives $\Lambda_\Gamma(u_\sigma)_1 = \Lambda_\Gamma(u_\sigma)_2$. Using the invertibility of Λ_Γ in Lemma 2.4, $(u_\sigma)_1 = (u_\sigma)_2 := u_\sigma$. This finally proves (3.7b).

This enables us to define on the whole domain Ω, u_{K} as equal to $(u_{\mathrm{K}})_j$ in subdomain Ω_j. A corresponding flux $F_{\mathrm{K},\sigma}$ for all edges which are not on the interface Γ is also identical to the subdomain flux. To characterize the finite volume problem in the whole domain, it remains to define the flux on an interface edge. Using (3.7b), it appears that (3.6) holds if for all $\sigma \in \boldsymbol{\mathcal{E}}_{\Gamma}, \sigma = \partial \mathrm{K}_1 \cap \partial \mathrm{K}_2$ with $\mathrm{K}_i \in \mathfrak{M}_i$,

$$F_{\mathrm{K},\sigma} = (F_{\mathrm{K}_1,\sigma})_1 = -(F_{\mathrm{K}_2,\sigma})_2. \tag{3.9}$$

Use the expression of the fluxes in (2.9), (2.10), for all $\sigma = \mathrm{K}_1 \cap \mathrm{K}_2 \in \boldsymbol{\mathcal{E}}_{\Gamma}$ and $\mathrm{K}_j \in \mathfrak{M}_j$, to obtain

$$\begin{aligned}
(F_{\mathrm{K}_1,\sigma})_1 &= \frac{|\sigma|\nu_\sigma}{d_{\mathrm{K}_1\sigma}}(u_{\mathrm{K}_1} - u_\sigma)(1 + B_{\mathrm{K}_1\sigma}) + \frac{1}{2}|\sigma| b_\sigma (u_{\mathrm{K}_1} + u_\sigma),\\
(F_{\mathrm{K}_2,\sigma})_2 &= \frac{|\sigma|\nu_\sigma}{d_{\mathrm{K}_2\sigma}}(u_{\mathrm{K}_2} - u_\sigma)(1 + B_{\mathrm{K}_2\sigma}) - \frac{1}{2}|\sigma| b_\sigma (u_{\mathrm{K}_2} + u_\sigma)
\end{aligned}$$

with $b_\sigma = b_{\mathrm{K}_1\sigma} = -b_{\mathrm{K}_2\sigma}$ and $B_{\mathrm{K}_j\sigma} = B_\sigma\big(\frac{b_{\mathrm{K}_j,\sigma} d_{\mathrm{K}_j\sigma}}{\nu_\sigma}\big)$. Equating $(F_{\mathrm{K}_1,\sigma})_1$ and $-(F_{\mathrm{K}_2,\sigma})_2$ provides

$$u_\sigma = \frac{\frac{|\sigma|\nu_\sigma}{d_{\mathrm{K}_1\sigma}}(1 + B_{\mathrm{K}_1\sigma})u_{\mathrm{K}_1} + \frac{|\sigma|\nu_\sigma}{d_{\mathrm{K}_2\sigma}}(1 + B_{\mathrm{K}_2\sigma})u_{\mathrm{K}_2} + \frac{1}{2} b_\sigma (u_{\mathrm{K}_1} - u_{\mathrm{K}_2})}{\frac{|\sigma|\nu_\sigma}{d_{\mathrm{K}_1\sigma}}(1 + B_{\mathrm{K}_1\sigma}) + \frac{|\sigma|\nu_\sigma}{d_{\mathrm{K}_2\sigma}}(1 + B_{\mathrm{K}_2\sigma})}.$$

Replace u_σ in the formula for $(F_{\mathrm{K}_1,\sigma})_1$ and rewrite it as

$$\begin{aligned}
(F_{\mathrm{K}_1,\sigma})_1 = \frac{\nu_\sigma|\sigma|}{d_\sigma} &\frac{\frac{d_\sigma}{d_{\mathrm{K}_1\sigma}}(1 + B_{\mathrm{K}_1\sigma})\frac{d_\sigma}{d_{\mathrm{K}_2\sigma}}(1 + B_{\mathrm{K}_2\sigma}) + \frac{1}{4}\big(\frac{d_\sigma b_\sigma}{\nu_\sigma}\big)^2}{\frac{d_\sigma}{d_{\mathrm{K}_1\sigma}}(1 + B_{\mathrm{K}_1\sigma}) + \frac{d_\sigma}{d_{\mathrm{K}_2\sigma}}(1 + B_{\mathrm{K}_2\sigma})} (u_{\mathrm{K}_1} - u_{\mathrm{K}_2})\\
&+ \frac{1}{2}|\sigma| b_\sigma (u_{\mathrm{K}_1} + u_{\mathrm{K}_2}).
\end{aligned}$$

Comparing with the formulation (2.10), it appears that (3.9) is realized (or equivalently that the solutions of (3.7) and (3.6) coincide) as soon as the flux $F_{\mathrm{K},\sigma}$ is defined by

$$\widetilde{B}_\sigma = \frac{\frac{d_\sigma}{d_{\mathrm{K}_1\sigma}}(1 + B_{\mathrm{K}_1\sigma})\frac{d_\sigma}{d_{\mathrm{K}_2\sigma}}(1 + B_{\mathrm{K}_2\sigma}) + \frac{1}{4}\big(\frac{d_\sigma b_\sigma}{\nu_\sigma}\big)^2}{\frac{d_\sigma}{d_{\mathrm{K}_1\sigma}}(1 + B_{\mathrm{K}_1\sigma}) + \frac{d_\sigma}{d_{\mathrm{K}_2\sigma}}(1 + B_{\mathrm{K}_2\sigma})} - 1, \tag{3.10}$$

$$F_{\mathrm{K},\sigma} = \frac{\nu_\sigma|\sigma|}{d_\sigma}(1 + \widetilde{B}_\sigma)(u_{\mathrm{K}_1} - u_{\mathrm{K}_2}) + \frac{1}{2}|\sigma| b_\sigma (u_{\mathrm{K}_1} + u_{\mathrm{K}_2}). \tag{3.11}$$

For each σ, by the assumptions on B_σ, the $B_{\mathrm{K}_j\sigma}$ are Lipschitz functions of $s = \frac{b_{\mathrm{K}_1,\sigma} d_{\mathrm{K}_1\sigma}}{\nu_\sigma}$ with $1 + B_\sigma \geq \underline{c}$. It is then easy to see that $\widetilde{B}_\sigma$ is also Lipschitz, that $1 + \widetilde{B}_\sigma \geq \frac{1}{2}\underline{c}$, and finally that

$$\widetilde{B}_\sigma(0) = \frac{\frac{d_\sigma}{d_{\mathrm{K}_1\sigma}}\frac{d_\sigma}{d_{\mathrm{K}_2\sigma}}}{\frac{d_\sigma}{d_{\mathrm{K}_1\sigma}} + \frac{d_\sigma}{d_{\mathrm{K}_2\sigma}}} - 1 = \frac{d_\sigma}{d_{\mathrm{K}_1\sigma} + d_{\mathrm{K}_2\sigma}} - 1 = 0.$$

Therefore (3.6) has a unique solution, which is also the solution of the limiting equations (3.7).

Second step: Convergence. By linearity, consider the convergence to 0 of the solution $\mathbf{u}^{\mathcal{T}_j,n} = (\mathbf{u}^{\mathfrak{M}_j,n}, \mathbf{u}^{\boldsymbol{\mathcal{E}}^j_\Gamma,n})$ of (3.4) when $f \equiv 0$. The proof technique is similar to the one used in Theorem 3.1.

We proceed as in Lemma 2.3: multiply (3.4a) by $(u_\kappa)^n_j$ and sum over all control volume $\kappa \in \mathfrak{M}_j$ to obtain

$$\sum_{\sigma\in\boldsymbol{\mathcal{E}}^j} \frac{|\sigma|\nu_\sigma}{d_\sigma}(1+B_\sigma)|u^{n,j}_\kappa - \widetilde{u}^{n,j}_\sigma|^2 + \int_{\Omega_j}\left(\eta + \frac{1}{2}\mathrm{div}\mathbf{b}\right)|u^{\mathfrak{M}_j,n}|^2 = -R^{n,j}_\Gamma \tag{3.12}$$

with

$$R^{n,j}_\Gamma = \sum_{\sigma\in\boldsymbol{\mathcal{E}}_\Gamma}(v_\sigma)^n_j\,(u_\sigma)^n_j, \quad (v_\sigma)^n_j := (F_{\kappa,\sigma})^n_j - \frac{1}{2}\int_\sigma \mathbf{b}\cdot\mathbf{n}_{\kappa\sigma}(u_\sigma)^n_j.$$

Since Λ_Γ is a symmetric positive definite linear operator on $\mathbb{R}^{\boldsymbol{\mathcal{E}}_\Gamma}$, its inverse Λ_Γ^{-1} can be defined, and it is also a symmetric positive definite operator on $\mathbb{R}^{\boldsymbol{\mathcal{E}}_\Gamma}$. Let $\|.\|_{\Lambda_\Gamma^{-1}}$ be the natural norm associated to this operator:

$$\|\mathbf{u}^{\boldsymbol{\mathcal{E}}_\Gamma}\|^2_{\Lambda_\Gamma^{-1}} = \langle\Lambda_\Gamma^{-1}(\mathbf{u}^{\boldsymbol{\mathcal{E}}_\Gamma}), \mathbf{u}^{\boldsymbol{\mathcal{E}}_\Gamma}\rangle_{\Lambda_\Gamma^{-1}} := \sum_{\sigma\in\boldsymbol{\mathcal{E}}_\Gamma}(\Lambda_\Gamma^{-1}(\mathbf{u}^{\boldsymbol{\mathcal{E}}_\Gamma}))_\sigma u_\sigma.$$

Now write

$$\begin{aligned} R^{n,j}_\Gamma &= \sum_{\sigma\in\boldsymbol{\mathcal{E}}_\Gamma}(v_\sigma)^n_j\Lambda_\Gamma^{-1}\Lambda_\Gamma(u_\sigma)^n_j = \left\langle(v_\sigma)^n_j, \Lambda_\Gamma(u_\sigma)^n_j\right\rangle_{\Lambda_\Gamma^{-1}} \\ &= \frac{1}{4}\left\|(v_\sigma)^n_j + \Lambda_\Gamma(u_\sigma)^n_j\right\|^2_{\Lambda_\Gamma^{-1}} - \frac{1}{4}\left\|(v_\sigma)^n_j - \Lambda_\Gamma(u_\sigma)^n_j\right\|^2_{\Lambda_\Gamma^{-1}}. \end{aligned}$$

Replace in (3.12) and sum over $n = 0, \ldots, N$, using assumption (2.11) to get, with a positive constant $\underline{\underline{C}}$,

$$\begin{aligned} &\underline{\underline{C}}\sum_{n=0}^{N}\sum_{j=1,2}\|u^{\mathfrak{M}_j,n}\|^2_{1,\mathfrak{M}_j} + \frac{1}{4}\sum_{j=1,2}\left\|(F_{\kappa,\sigma})^N_j - \frac{1}{2}\int_\sigma \mathbf{b}\cdot\mathbf{n}_{\kappa\sigma}(u_\sigma)^N_j + \Lambda_\Gamma(u_\sigma)^N_j\right\|^2_{\Lambda_\Gamma^{-1}} \\ &\le \frac{1}{4}\sum_{j=1,2}\left\|(F_{\kappa,\sigma})^0_j - \frac{1}{2}\int_\sigma \mathbf{b}\cdot\mathbf{n}_{\kappa\sigma}(u_\sigma)^0_j + \Lambda_\Gamma(u_\sigma)^0_j\right\|^2_{\Lambda_\Gamma^{-1}}. \end{aligned}$$

This yields the convergence of the sequence $u^{\mathfrak{M}_j,n}$ toward 0 in the discrete H^1 norm and completes the proof of the theorem. □

Given an approximation (3.6) on a composite mesh $\mathcal{T}$, the inverse question is whether it is possible to construct a discrete Schwarz algorithm that converges toward (3.6). An answer to this question is given in the next theorem.

THEOREM 3.3. *Consider in* (3.6) *the convective discrete fluxes defined by constant flux* $\widetilde{B}_\sigma := \widetilde{B}$ *for all* $\sigma \in \boldsymbol{\mathcal{E}}$, *where* $\widetilde{B}$ *satisfies* (2.11) *and the additional condition*

$$\widetilde{B}(s) > -1 + \frac{1}{2}|s|. \tag{3.13}$$

Redefine for all $\sigma \in \boldsymbol{\mathcal{E}}_\Gamma$ the distance $d_{\mathrm{K}_j,\sigma} = \frac{1}{2}d_\sigma$ (see Figure 3), and define the discrete convective fluxes in the Schwarz algorithm (3.4) *by*

(3.14)
$$B_\sigma(s) = \begin{cases} \widetilde{B}(s) & \text{if } \sigma \notin \boldsymbol{\mathcal{E}}_\Gamma, \\ B(s) := -\frac{1}{2}\big(1 - \widetilde{B}(2s)\big) + \frac{1}{2}\sqrt{(1 - s + \widetilde{B}(2s))(1 + s + \widetilde{B}(2s))} & \text{if } \sigma \in \boldsymbol{\mathcal{E}}_\Gamma. \end{cases}$$

Then B_σ is a new admissible flux in the sense of (2.11)*, and* (3.6) *is the limit of the Schwarz algorithm* (3.4)*.*

Proof. By the proof of Theorem 3.2 above, (3.6) is the limit of the Schwarz algorithm (3.4) if and only if (3.10) holds for any $\sigma \in \boldsymbol{\mathcal{E}}_\Gamma$. Since B_σ is even, the assumption $d_{\mathrm{K}_j,\sigma} = \frac{1}{2}d_\sigma$ implies that $B_{\mathrm{K}_1\sigma} = B_{\mathrm{K}_2\sigma} = B_\sigma(s)$ for $s = \frac{b_\sigma d_\sigma}{2\nu_\sigma}$. Then (3.10) can be rewritten as

$$\widetilde{B}(2s) = B(s) + \frac{\frac{1}{4}s^2}{1 + B(s)}\,. \tag{3.15}$$

Given s and $\widetilde{B}(2s)$, this yields a second degree equation for $B(s)$,

$$X^2 + (1 - \widetilde{B}(2s))X + \frac{1}{4}s^2 - \widetilde{B}(2s) = 0,$$

whose only solution satisfying $B(0) = 0$ is given by (3.14). It is then easy to see that B is an even Lipschitz function of s and that

$$1 + B_\sigma(s) \geq \begin{cases} 1 + \widetilde{B}(s) & \text{if } \sigma \notin \boldsymbol{\mathcal{E}}_\Gamma \\ \frac{1}{2}(1 + \widetilde{B}(2s)) & \text{if } \sigma \in \boldsymbol{\mathcal{E}}_\Gamma \end{cases} \geq \frac{1}{2}(1 + \underline{c}).$$

In that sense, it is a new admissible flux in the sense of (2.11). ∎

Remark 3.4. Assumption (3.13) is satisfied by the upwind scheme, the Scharfetter–Gummel scheme, and the centerd scheme provided $|s| < 1$. The Scharfetter–Gummel scheme, as described in [6], is obtained by computing the fluxes such that the solution on the line $(\boldsymbol{x}_\mathrm{K}, \boldsymbol{x}_\mathrm{L})$ of the boundary problem $-\frac{\nu_\sigma}{d_\sigma}\tilde{u}'(\theta) + b_{\mathrm{K}\sigma}\tilde{u}(\theta) = \frac{1}{|\sigma|}F_{\mathrm{K},\sigma} = -\frac{1}{|\sigma|}F_{\mathrm{L},\sigma}$, $\tilde{u}(0) = u_\mathrm{K}$ with $\tilde{u}(\theta) = u(\boldsymbol{x}_\mathrm{K} + \theta(\boldsymbol{x}_\mathrm{L} - \boldsymbol{x}_\mathrm{K}))$ satisfies $\tilde{u}(1) = u_\mathrm{L}$. It seems to be particularly well adapted for the Schwarz algorithm with the assumption of Theorem 3.3, since in that case $\widetilde{B}_\sigma = B_\sigma$ as depicted in Figure 5. Figure 5 shows in the other cases that the new convective flux adds more diffusion on the interface.

Remark 3.5. The a priori estimate in Theorem 2.7 requires some geometrical properties of the domain through the Poincaré inequality that we implicitly use. The extended Poincaré inequality proved in [6] only requires connectedness of the domain. There is an example in [4] of the application of a Robin–Schwarz algorithm with improved finite volume (DDFV) discretization in the case of a nonconvex domain.

4. Numerical experiments. The aim of this section is first to evaluate numerically the accuracy of the schemes introduced in section 2 and second to evaluate the efficiency of the Ventcell–Schwarz algorithm compared to Robin–Schwarz. The domain $\Omega =]-1, 1[\times]0, 1[$ is split into $\Omega_1 =]-1, 0[\times]0, 1[$ and $\Omega_2 =]0, 1[\times]0, 1[$ with an interface Γ at $x = 0$.

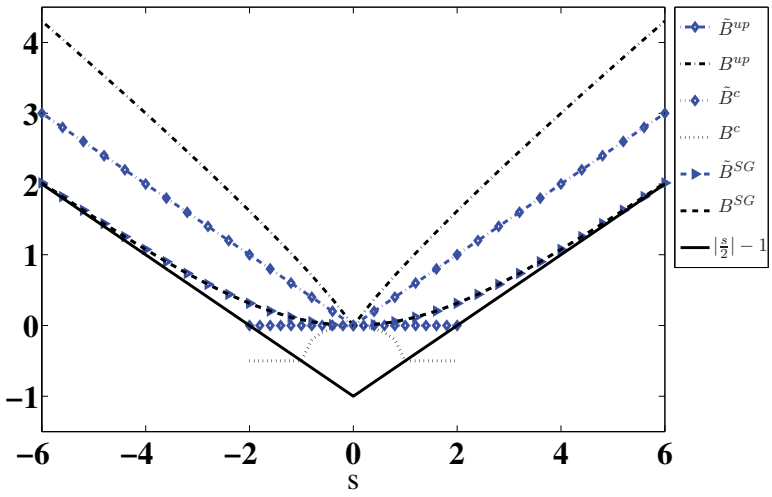

FIG. 5. *The different functions* $\widetilde{B}$ *and* B *in* (3.14).

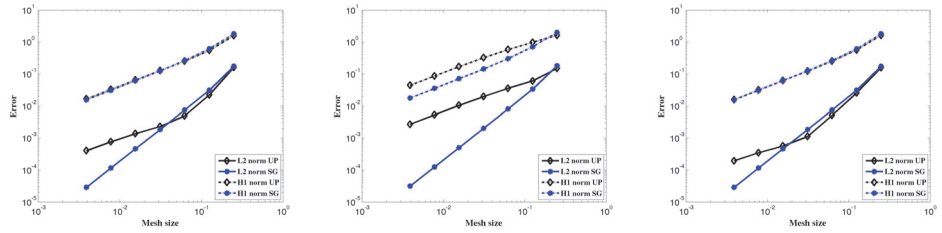

(a) $\mathbf{b} = \mathbf{b}_1$ (b) $\mathbf{b} = \mathbf{b}_2$ (c) $\mathbf{b} = \mathbf{b}_3$

FIG. 6. *Comparison of the accuracy for various choices of the discrete flux* B.

The diffusion and reaction parameters are fixed equal to $\nu = 0.1$, $\eta = 1$. Three different advection terms are investigated. The first corresponds to balancing advection and diffusion, the second to an advection-dominated problem, and the third to rotating advection:

$$\mathbf{b}_1(x,y) = \begin{pmatrix} 1 \\ 1 \end{pmatrix}, \quad \mathbf{b}_2(x,y) = \begin{pmatrix} 10 \\ 1 \end{pmatrix}, \quad \mathbf{b}_3(x,y) = \begin{pmatrix} -\cos(\pi x)\sin(\pi y) \\ \sin(\pi x)\cos(\pi y) \end{pmatrix}.$$

The source f is such that the exact solution of (1.1) is $u(x,y) = \sin(3\pi x)\sin(3\pi y)$.

4.1. Accuracy of the scheme with Ventcell boundary condition. We illustrate here the convergence behavior of (2.16), (2.17) in Ω_2, with Ventcell boundary condition on Γ for given coefficients $p = q = 1$.

In Figure 6 the accuracy of upwind and Scharfetter–Gummel schemes is compared in the discrete L^2 and H^1 norms. The centerd and Scharfetter–Gummel schemes give close results; therefore only one of them is represented. This is due to the facts that for fine meshes $\frac{b_{K\sigma} d_\sigma}{\nu_\sigma} \ll 1$ and that $B^{SG}(s) - B^c(s) = \mathcal{O}(s^2)$ in the neighborhood of $s = 0$. The errors produced by the Scharfetter–Gummel and upwind schemes are relatively close in the H^1 norm, bounded respectively by $C^{SG}\text{size}(\mathfrak{M})$ and $C^{up}\text{size}(\mathfrak{M})$ with $C^{SG} \leq C^{up}$. If the error is measured in the L^2 norm, however, a superconvergence effect occurs for the Scharfetter–Gummel scheme, that is, an error $\mathcal{O}(\text{size}(\mathfrak{M})^2)$. In

the case of dominating advection $\mathbf{b} = \mathbf{b}_2$, the Scharfetter–Gummel scheme is clearly a better approximation for both coarse and fine grids.

4.2. Convergence behavior of the Schwarz algorithm. We compare in this paragraph the convergence behavior of the optimized Schwarz algorithm for Robin and Ventcell transmission conditions. Asymptotic values for the parameters were obtained in [9] for $\Omega = \mathbb{R}$, and $\Omega_j = \mathbb{R}_\pm$, as follows. By a Fourier transform in the second variable, a local convergence factor is defined, and the convergence factor of the algorithm is defined as the maximum in absolute value over all frequencies which would be present in the solution if it were represented on a grid of size h. Optimal parameters p and q are computed asymptotically so as to minimize the convergence factor and given by

$$\text{Robin:} \quad p^\star = \frac{1}{2} h^{-\frac{1}{2}} \sqrt{2\pi\nu (b_x^2 + 4\nu\eta)^{\frac{1}{2}}}, \quad q^\star = 0, \tag{4.1}$$

$$\text{Ventcell:} \quad p^\star = \frac{h^{-\frac{1}{4}}}{2} \sqrt[4]{\frac{\nu\pi (b_x^2 + 4\nu\eta)^{\frac{3}{2}}}{2}}, \quad q^\star = \frac{h^{\frac{3}{4}}}{2} \sqrt[4]{\frac{8\nu}{\pi^3}} (b_x^2 + 4\nu\eta)^{-\frac{1}{2}}. \tag{4.2}$$

The corresponding theoretical convergence factor of the algorithm (i.e., the factor of reduction of the L^2 norm of the error in one iteration) is

$$\text{Robin: } \rho^\star = 1 - \mathcal{O}(h^{\frac{1}{2}}), \quad \text{Ventcell: } \rho^\star = 1 - \mathcal{O}(h^{\frac{1}{4}}), \tag{4.3}$$

showing a drastic theoretical asymptotic improvement from Robin to Ventcell, since it is less dependent on the size of the mesh.

The value of b_x in the formula is $\mathbf{b} \cdot \mathbf{n}$ when the advection is constant along the interface. In the case of variable advection $\mathbf{b} = \mathbf{b}_3$, the choice of b_x is the mean value along Γ of the function $\mathbf{b} \cdot \mathbf{n}$. We have tested a local choice for these parameters as well, but the convergence seems to be slightly improved by this global choice.

We illustrate our results on the two families of triangular grids presented in Figure 7, one conforming (Grid # 1), the other nonconforming (Grid # 2) at the

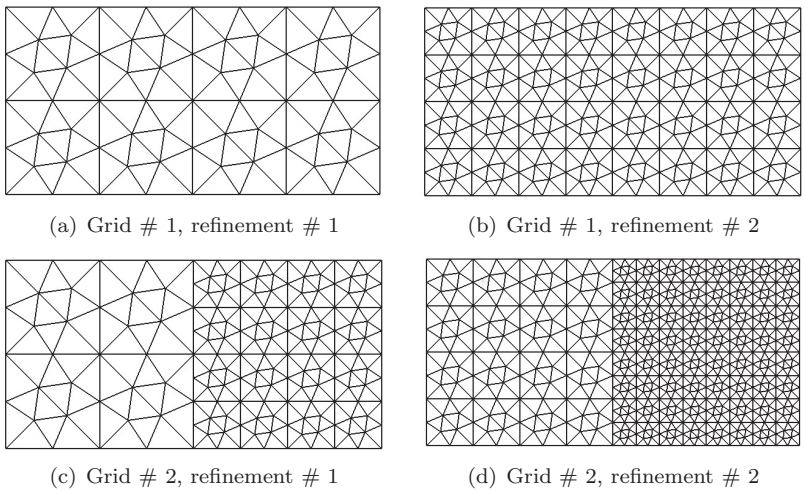

(a) Grid # 1, refinement # 1 (b) Grid # 1, refinement # 2

(c) Grid # 2, refinement # 1 (d) Grid # 2, refinement # 2

FIG. 7. *The two families of meshes. The family Grid # 1 is an example of triangular meshes conformal at the interface $x = 0$. The family Grid # 2 is an example of triangular meshes with nonconformal edges at the interface $x = 0$.*

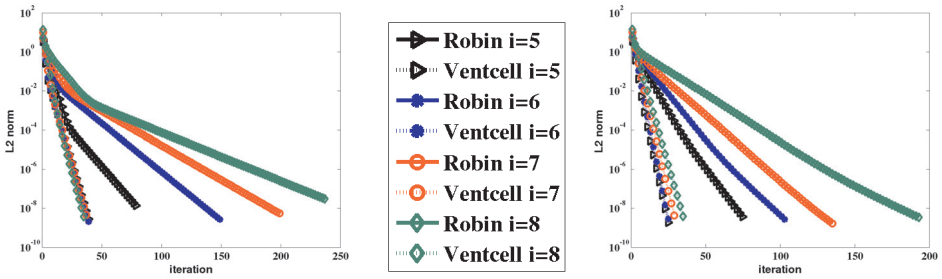

FIG. 8. *L^2 norm error w.r.t. iterations for increasing mesh refinements for Scharfetter–Gummel approximation and* $\mathbf{b} = \mathbf{b}_1$. *Left: Grid # 1. Right: Grid # 2.*

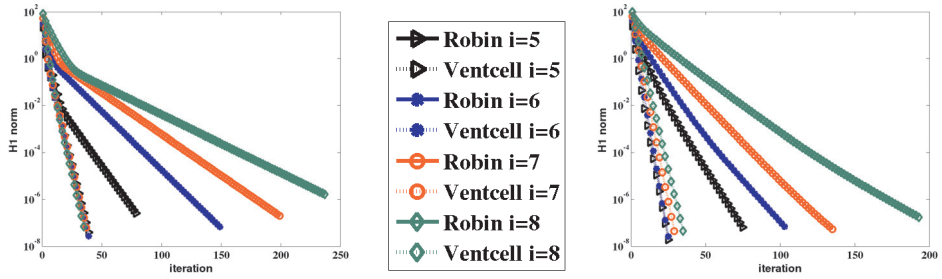

FIG. 9. *H^1 norm error w.r.t. iterations for increasing mesh refinements for Scharfetter–Gummel approximation and* $\mathbf{b} = \mathbf{b}_1$. *Left: Grid # 1. Right: Grid # 2.*

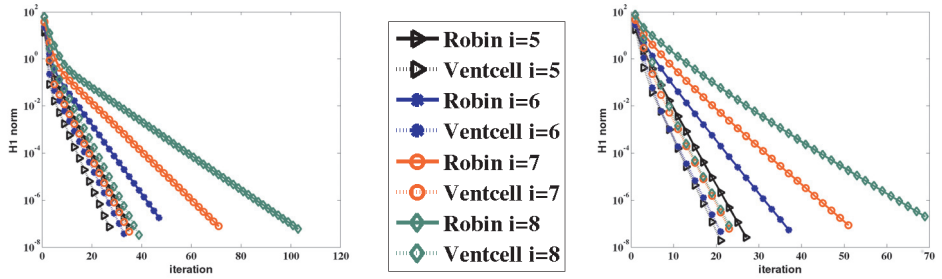

FIG. 10. *H^1 norm error w.r.t. iterations for increasing mesh refinements for Scharfetter–Gummel approximation and* $\mathbf{b} = \mathbf{b}_2$. *Left: Grid # 1. Right: Grid # 2.*

interface Γ. We refer to [16] for examples on square grids. Figures 8–12 show the convergence history for increasing mesh refinement, defined by the parameter $i = 3, 4, 5, 6$. The algorithm is stopped as soon as $\|u^{\mathcal{T},n+1} - u^{\mathcal{T},n}\|_{H^1} \leq 10^{-7}$. The experiments show that the choice of the distance $d_{\mathrm{K},\sigma}$ has a low impact on the convergence, and therefore we have chosen $d_{\mathrm{K},\sigma} = d^{\perp}_{\mathrm{K},\sigma}$ in Figures 8–12.

4.3. Comparison of Robin– and Ventcell–Schwarz algorithms for the Scharfetter–Gummel scheme. Figures 8 and 9 display the convergence history in the L^2 norm and H^1 norm, respectively, for the advection $\mathbf{b} = \mathbf{b}_1$.

Figures 10 and 11 display the convergence history in the H^1 norm for the advection vectors $\mathbf{b} = \mathbf{b}_2$ and $\mathbf{b} = \mathbf{b}_3$.

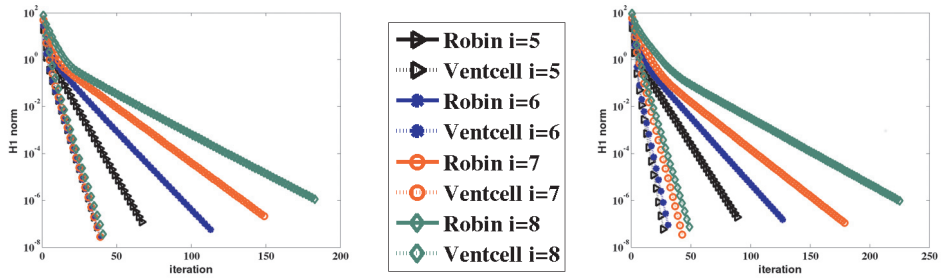

FIG. 11. *H^1 norm error w.r.t. iterations for increasing mesh refinements for Scharfetter–Gummel approximation and* $\mathbf{b} = \mathbf{b}_3$. *Left: Grid # 1. Right: Grid # 2.*

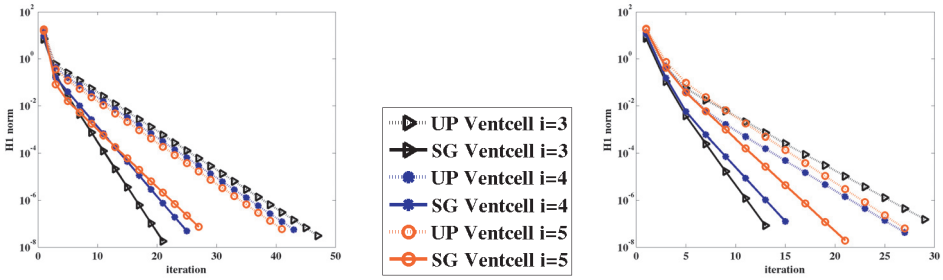

FIG. 12. *H^1 norm error w.r.t. iterations for increasing mesh refinements. Comparison between the upwind scheme and the Scharfetter–Gummel scheme for* $\mathbf{b} = \mathbf{b}_2$. *Left: Grid # 1. Right: Grid # 2.*

TABLE 1
Robin versus Ventcell. The values of α in the case of Scharfetter–Gummel scheme L^2 norm.

	Grid # 1			Grid # 2		
α	$\mathbf{b}_1$	$\mathbf{b}_2$	$\mathbf{b}_3$	$\mathbf{b}_1$	$\mathbf{b}_2$	$\mathbf{b}_3$
Robin	0.47	0.43	0.47	0.45	0.40	0.49
Ventcell	-0.02	0.06	0.01	0.08	0.04	0.20

Note that the case $\mathbf{b} = \mathbf{b}_2$ (advection-dominated case) requires a finer mesh, able to capture the advection. Therefore we have considered refinements up to eight times. For the various types of advection, for conforming or nonconforming meshes, the gain of using the Ventcell transmission condition is spectacular: the convergence is faster and hardly dependent on the mesh size. The behaviors in the L^2 norm or H^1 norm are very similar. Furthermore the Ventcell–Schwarz algorithm behaves much better for nonconforming grids than the Robin–Schwarz.

The slopes of the convergence curves in the figures above, for different values of the mesh size, provide a coefficient α in the discrete convergence factor $\rho_d \sim 1 - Ch^\alpha$, to be compared to 1/2 and 1/4 in (4.3). These coefficients are given in Table 1. They are even better than the theoretical ones. For all types of advection, even in the nonconforming case, the numerical convergence factors are almost independent of the mesh size.

Concerning a discrete analysis of convergence, a general argument in [18] in the finite element framework asserts that if $p = \mathcal{O}(h^{-\frac{1}{4}})$ and $q = \mathcal{O}(h^{\frac{3}{4}})$, the spectral radius of the iteration matrix is $1 - \mathcal{O}(h^{\frac{1}{4}})$. However, in the finite volumes framework, special care should be given to the treatment of the boundary operator; see [13]. The

ideas in these two papers could be coupled to produce a discrete convergence factor for our algorithm.

4.4. Comparison of two discretization schemes. All the results above are asymptotic results when the mesh size is small. Figure 12 displays the convergence history when using the upwind scheme and the Scharfetter–Gummel scheme for $\mathbf{b} = \mathbf{b}_2$ with a coarse mesh. The approximate values are those in (4.2), and these plots show that these coefficients are still relevant, even though the dependency in h is not perfect.

We saw in Figure 6 that for the advection-dominated problem, the Scharfetter–Gummel scheme is more accurate than the upwind scheme. We furthermore see here that associated to a Schwarz algorithm, the convergence is also much faster than for the upwind scheme, especially for coarse grids.

5. Conclusion. We have introduced and analyzed a new nonoverlapping domain decomposition algorithm for finite volume approximation of the advection-diffusion equation in two dimensions. It relies on the Ventcell transmission condition and converges much faster than when using the Robin condition. Only continuous coefficients were considered for simplicity, but the extension to discontinuous viscosity across the interface can easily be done. In the case of strong anisotropy, it will be interesting to use more versatile schemes such as DDFV schemes, in the spirit of [4] and [13]. The computation of order 2 optimized parameters is a great challenge in that case. Extension to three dimensions should be forthcoming in the case of admissible finite volume three-dimensional meshes, as the analysis of the three-dimensional FV4 schemes does not bring additional difficulties (see [10, 12]). Admissibility in the finite volume sense though induces restrictions on the meshes. One way to overcome these restrictions is to use the above-mentioned more evolved DDFV schemes. The three-dimensional extension of DDFV Schwarz algorithm using one of the three-dimensional DDFV schemes (see [3, 2, 8]) will be a substantial improvement.

Acknowledgments. The authors would like to thank the anonymous referees for many valuable comments. Special thanks to Juliet Ryan from ONERA, who greatly helped the presentation of the paper.

REFERENCES

[1] Y. Achdou, C. Japhet, F. Nataf, and Y. Maday, *A new cement to glue non-conforming grids with Robin interface conditions: The finite volume case*, Numer. Math., 92 (2002), pp. 593–620.

[2] B. Andreianov, M. Bendahmane, and F. Hubert, *On 3D DDFV discretization of gradient and divergence operators.* II. *Discrete functional analysis tools and applications to degenerate parabolic problems*, Comput. Methods Appl. Math., 13 (2013), pp. 369–410.

[3] B. Andreianov, M. Bendahmane, F. Hubert, and S. Krell, *On 3D DDFV discretization of gradient and divergence operators.* I. *Meshing, operators and discrete duality.*, IMA J. Numer. Anal., 32 (2012), pp. 1574–1603.

[4] F. Boyer, F. Hubert, and S. Krell, *Non-overlapping Schwarz algorithm for solving 2D m-DDFV schemes*, IMA J. Numer. Anal., 30 (2009), pp. 1062–1100.

[5] R. Cautrès, R. Herbin, and F. Hubert, *The Lions domain decomposition algorithm on non-matching cell-centred finite volume meshes*, IMA J. Numer. Anal., 24 (2004), pp. 465–490.

[6] C. Chainais-Hillairet and J. Droniou, *Finite volume schemes for non-coercive elliptic problems with Neumann boundary conditions*, IMA J. Numer. Anal., 31 (2011), pp. 61–85.

[7] C. Chniti, F. Nataf, and F. Nier, *Improved interface conditions for 2D domain decomposition with corners: A theoretical determination*, Calcolo, 45 (2008), pp. 111–147.

[8] Y. Coudière and F. Hubert, *A 3D discrete duality finite volume method for nonlinear elliptic equation*, SIAM J. Sci. Comput., 33 (2011), pp. 1739–1764.

[9] O. Dubois, *Optimized Schwarz Methods for the Advection-Diffusion Equation and for Problems with Discontinuous Coefficients*, Ph.D. thesis, McGill University, Montréal, Canada, 2007.

[10] R. Eymard, T. Gallouët, and R. Herbin, *Finite Volume Methods*, in Techniques of Scientific Computing, Handb. Numer. Anal. 7, North-Holland, Amsterdam, 2000, pp. 713–1020.

[11] C. G. Gal, *A Cahn-Hilliard model in bounded domains with permeable walls*, Math. Methods Appl. Sci., 29 (2006), pp. 2009–2036.

[12] T. Gallouët, R. Herbin, and M. H. Vignal, *Error estimates on the approximate finite volume solution of convection diffusion equations with general boundary conditions*, SIAM J. Numer. Anal., 37 (2000), pp. 1935–1972.

[13] M. J. Gander, F. Hubert, and S. Krell, *Optimized Schwarz algorithms in the framework of DDFV schemes*, in Proceedings of the 21st International Conference on Domain Decomposition Methods, Rennes, 2012.

[14] M. J. Gander, C. Japhet, Y. Maday, and F. Nataf, *A new cement to glue nonconforming grids with Robin interface conditions: The finite element case*, in Domain Decomposition Methods in Science and Engineering, Lecture Notes in Comput. Sci. Engrg. 40, Springer, New York, 2005, pp. 259–266.

[15] G. R. Goldstein, *Derivation and physical interpretation of general boundary conditions*, Adv. Differential Equations, 11 (2006), pp. 457–480.

[16] L. Halpern and F. Hubert, *A finite volume Ventcell-Schwarz algorithm for advection-diffusion equations*, in Proceedings of the 21st International Conference on Domain Decomposition Methods, Rennes, 2012.

[17] C. Japhet, *Méthode de décomposition de domaine et conditions aux limites artificielles en mécanique des fluides: méthode Optimisée d'Ordre* 2 *(OO*2*)*, Ph.D. thesis, Université Paris 13, France, 1998; also available online from http://tel.archives-ouvertes.fr/tel-00558701/fr/.

[18] S. H. Lui, *Convergence estimates for an higher order optimized Schwarz method for domains with an arbitrary interface*, J. Comput. Appl. Math., 235 (2010), pp. 301–314.

[19] J. Szeftel, *Calcul pseudo-différentiel et para-différentiel pour l'étude des conditions aux limites absorbantes et des propriétés qualitatives des EDP non linéaires*, Ph.D. thesis, Université Paris 13, France, 2004; also available online from http://www.math.ens.fr/∼szeftel/these.pdf.

[20] A. D. Ventcel′, *On boundary conditions for multi-dimensional diffusion processes*, Theory Probab. Appl., 4 (1959), pp. 164–177.